nature reviews neurology

https://doi.org/10.1038/s41582-022-00753-3

Review article

Check for updates

Functional brain networks in the evaluation of patients with neurodegenerative disorders

Matej Perovnik[1,2,4], Tomaž Rus[1,2,4], Katharina A. Schindlbeck[3] & David Eidelberg[3]

Abstract

Network analytical tools are increasingly being applied to brain imaging maps of resting metabolic activity (PET) or blood oxygenation-dependent signals (functional MRI) to characterize the abnormal neural circuitry that underlies brain diseases. This approach is particularly valuable for the study of neurodegenerative disorders, which are characterized by stereotyped spread of pathology along discrete neural pathways. Identification and validation of disease-specific brain networks facilitate the quantitative assessment of pathway changes over time and during the course of treatment. Network abnormalities can often be identified before symptom onset and can be used to track disease progression even in the preclinical period. Likewise, network activity can be modulated by treatment and might therefore be used as a marker of efficacy in clinical trials. Finally, early differential diagnosis can be achieved by simultaneously measuring the activity levels of multiple disease networks in an individual patient's scans. Although these techniques were originally developed for PET, over the past several years analogous methods have been introduced for functional MRI, a more accessible non-invasive imaging modality. This advance is expected to broaden the application of network tools to large and diverse patient populations.

Sections

[1]Department of Neurology, University Medical Center Ljubljana, Ljubljana, Slovenia. [2]Medical Faculty, University of Ljubljana, Ljubljana, Slovenia. [3]Center for Neurosciences, The Feinstein Institutes for Medical Research, Manhasset, NY, USA. [4]These authors contributed equally: Matej Perovnik, Tomaž Rus. e-mail: deidelberg@northwell.edu

Key points

- Parkinson disease, Alzheimer disease and other neurodegenerative disorders are characterized by specific disease-related functional topographies (brain networks) that can be identified and validated using metabolic PET or resting-state functional MRI.
- Brain network activity can be quantified on an individual patient basis, and the resulting network expression levels can be used in research and clinical settings.
- Expression levels for multiple disease-related topographies can be entered into computational algorithms used to classify patients according to the diagnostic likelihood of these diseases.
- Expression levels for abnormal disease networks correlate with clinical symptom severity and can be modulated by effective treatment.
- Network expression levels increase over time and can be used to predict the likelihood of transition from preclinical to symptomatic disease in at-risk individuals.
- The characterization of treatment-induced networks opens the door to their future use as objective outcome measures in clinical trials.

Introduction

Neurodegenerative brain disorders are among the leading causes of disability in elderly populations (age >75 years) worldwide[1,2]. In total, in 2019, approximately 57 million people were living with dementia, as well as 8.5 million with parkinsonism[2,3]. The prevalence of these disorders has risen markedly in the past three decades. Indeed, since 1990, substantial increases have occurred in the prevalence of dementia (117%) and Parkinson disease (PD) (74%), leading to increased health-care costs and societal burden, which are projected to grow further[1,4–7]. Treatment options are currently symptomatic only, but disease-modifying therapies to slow down or halt the underlying pathological processes are an important focus of drug development[8,9]. Accurate diagnosis is necessary for the success of experimental trials of new treatments for neurodegenerative brain disorders. That said, diagnosis of common neurodegenerative disorders on clinical grounds alone is only moderately accurate (70–80%)[10–14]. Although histopathological examination of brain tissue still represents the gold standard for diagnosis, detailed understanding of the involved molecular and anatomical pathways and the use of in vivo biomarkers to support reliable, early diagnosis are gaining importance in some disorders[15,16].

Over the past decade, neuroimaging research has transitioned from mapping local effects to developing predictive models of neural activity that integrate information distributed across multiple brain systems in health and disease[17,18]. Multivariate pattern analyses of brain activity based on principal component analysis (PCA) are data driven and can be designed to discriminate one category from another in the absence of prespecified regions of interest (such as diseased versus healthy states, or a disease from a clinically similar syndrome), evaluate individual differences in behaviour or test performance (including cognitive functioning in healthy individuals or in a specific population of patients) and assess the effects of disease and/or treatment over time (for example, to compare patients receiving an active drug treatment with those receiving a placebo in randomized clinical trials). Various imaging modalities have been used to identify and evaluate functional brain network patterns: metabolic imaging with [^{18}F]fluorodeoxyglucose (FDG) PET; perfusion imaging-based mapping of local cerebral blood flow using $H_2{}^{15}O$ PET, single-photon emission CT (SPECT) or early-phase dynamic PET with ^{18}F-labelled radiotracers[19]; non-invasive MRI techniques such as resting-state (rs) functional MRI (fMRI), which records fluctuations in local blood oxygen-level dependent (BOLD) signals, as well as arterial spin-labelled (ASL) MRI to map regional cerebral blood flow. Functional neuroimaging maps of cerebral glucose metabolism and blood flow generally provide complementary information owing to neurovascular coupling[20], which is present under normal conditions and most pathological conditions. That said, these two measures can be uncoupled in some disease states, such as ischaemic stroke, traumatic brain injury and glioma[21–23] as well as under specific treatment conditions. For instance, in patients with PD, levodopa administration induces dissociation of blood flow and glucose metabolism in dopaminoceptive PD-related motor network regions, leading to substantial neurovascular uncoupling[24,25]. Despite their methodological differences, these imaging modalities have all been used in prospective studies for the quantitative evaluation of disease networks. Indeed, the clinical utility of multivariate approaches to brain imaging and network quantification is derived from this approach, which is termed topographic profile rating (Box 1).

In this Review, we summarize advances in network analysis of brain images in patients with neurodegenerative disorders, including PD, Alzheimer disease, dementia with Lewy bodies (DLB) and frontotemporal dementia (FTD). We focus on techniques that detect and validate disease-specific networks and consider the relationship of these networks to the underlying pathological processes and disease-related genotypes. In addition, we discuss the findings of studies that used graph analysis to describe the stereotyped changes in internal network organization that can occur in these disorders. Last, we discuss the potential clinical applications of brain network analysis: to enhance diagnostic accuracy, predict functional decline, track disease progression and monitor treatment effects.

Functional brain network mapping

Multivariate algorithms

Univariate algorithms have been widely used to localize regional abnormalities of brain function[26], but these techniques focus on voxel-by-voxel comparisons and do not explicitly consider the relationships between spatially distributed clusters[27]. By contrast, multivariate analyses focus specifically on these relationships and can be used to identify sources of disease-related variation in imaging data[27–30]. Multivariate analysis has been used in FDG PET-based studies of metabolic connectivity, and various methods have been used to extract brain network information from patient scan data[31–33]. Importantly, approaches such as PCA[34] enable the characterization of covariance topographies that are strongly associated with disease states while facilitating the biological interpretation of scan data through dimensionality reduction[27,33]. One of the most popular PCA-based algorithms used to study brain disorders is the scaled subprofile model (SSM)[27,29,30] (Box 1). A related approach based on supervised PCA, termed ordinal trend analysis (OrT, a form of canonical variates analysis (CVA)) was subsequently developed to handle within-individual network changes across experimental conditions[35], as occurs in disease progression and in therapeutic trials[36–40]. In either approach, the derived networks must be validated by prospective

Box 1

Metabolic brain network pattern identification

Principal component (PC) analysis (PCA) is a statistical method used to reduce dimensionality by creating new, uncorrelated variables that account for the maximal variance in the data[34]. The scaled subprofile model (SSM) is a PCA-based method[28–30] that enables the identification of disease-related spatial covariance topographies[27,33,116]. SSM–PCA of brain scans from a combined group of patients (in this example, with Parkinson disease (PD)) and healthy control individuals, unbiased by clinical category, results in one or more linearly independent (that is, orthogonal) spatial covariance patterns termed PCs. The PCs explain a considerable portion of the subject-by-region (voxel) variance in the imaging data and demonstrate maximal differences in expression level (subject scores or PC scalars) between patients and controls. In brief, to identify a stable disease-related pattern, 10–20 scans from patients and a similar number of scans from age-matched and sex-matched healthy control individuals are analysed. During preprocessing, each scan is spatially normalized and smoothed (not shown) and then (step **1**) transformed into a subject-by-voxel data matrix (for convenience, this step is depicted using regions of interest (ROIs) instead of voxels). Grey matter is extracted using count thresholding or by applying a customized mask. The remaining voxels are logarithmically transformed (step **2**) and the matrix is double-centred by subtracting row and column means to yield the subject residual profile (SRP). PCA is applied to the subject-by-voxel covariance matrix to obtain subject score vectors (step **3**) with associated eigenvalues and PCs (step **4**). The top PCs are selected and entered into a series of logistic regression models used to classify scans according to their expression levels (subject scores) for each of the selected PCs, singly or in combination. The model with the lowest Akaike information criterion (step **5**) is selected as a disease-related network (step **6**).

Further steps are required to confirm the validity and biological significance of a disease-related network. The stability of voxel weights can be tested using either bootstrapping or leave-one-out cross-validation methods[27,33]. Disease-related network expression is prospectively validated in independent patient cohorts. This computational procedure is termed topographic profile rating (TPR), in which subject scores are calculated as the dot product of the pattern vector with the SRP[27]. The resulting values quantify pattern expression in individual cases and have been used extensively to assess disease progression[39,125,126] and for differential diagnosis[143,145,155,178]. The prognostic value of TPR has been demonstrated for conversion to Alzheimer disease in patients with mild cognitive impairment[184] and conversion to PD or dementia with Lewy bodies in patients with rapid eye movement sleep behaviour disorder[118]. However, currently no studies have explored the value of TPR in predicting conversion to PD or dementia with Lewy bodies in patients with mild cognitive impairment. PDRP, PD-related pattern.

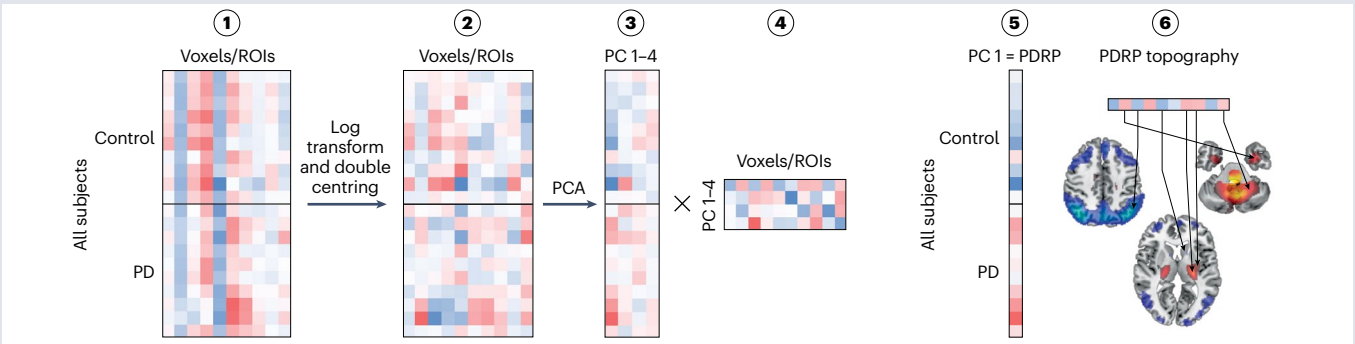

testing in an independent dataset (that is, scans that were not used in the pattern-identification stage).

Metabolic PET versus rs-fMRI

The integration of multimodal data from brain imaging studies can provide relevant information on network function, particularly in individuals with neurodegenerative disorders. Regional glucose metabolism in the brain as assessed with FDG PET is coupled to local synaptic activity[41–43], although some evidence suggests that inflammatory responses in neighbouring microglia can contribute to an increased glucose utilization signal under pathological conditions[44]. Whereas FDG PET yields autoradiographic images of brain metabolic activity measured over minutes, rs-fMRI records transient haemodynamic fluctuations in blood oxygenation in the form of a BOLD signal, which is coupled to neuronal activity[20,45,46]. Nonetheless, because rs-fMRI is sensitive to events that occur in a much shorter time window than FDG PET, rs-fMRI and FDG PET might extract different, although perhaps complementary, regional relationships[47–49].

In FDG PET, covariance topographies are identified through classical matrix decomposition algorithms, by which large arrays of ordered rows and columns representing scan data are reduced to a smaller set of statistically significant components[27,28]. In rs-fMRI, the extraction of discrete networks relies on relationships between BOLD signal time series recorded in key regions. To this end, seed-based approaches assess correlations between time series (or their Fourier transforms) measured in a prespecified 'seed' region and activity recorded in other regions or

voxel clusters[50,51]. Covariance methods such as PCA are not optimal for application to spatiotemporal data, such as those provided by BOLD signals. That said, methods of blind source separation, such as independent component analysis (ICA), provide a data-driven algorithm to disambiguate independent source signals in rs-fMRI data[52]. As in PCA, ICA seeks to extract discrete multiregional components from scan data. However, unlike PCA and other correlation-based methods, ICA correlates the signals while reducing higher-order statistical dependencies. Thus, ICA identifies signals that are maximally independent, whereas PCA identifies the set of one or more linearly independent topographic patterns (orthogonal eigenvectors) that accounts for the greatest variance in the data. ICA has been used to study functional connectivity in groups as well as in individual patients[53,54]. Indeed, a strategy analogous to that employed with SSM–PCA has been developed, in which ICA was used to identify and validate reproducible disease networks in rs-fMRI data from patients with PD[55,56] (Box 2). Indeed, similar network topographies have been characterized using either FDG PET or rs-fMRI data from patients with neurodegenerative disorders[56–59].

Network assessment with graph theory

Multivariate approaches such as PCA and ICA provide important information about the specific regional elements (or 'nodes') that comprise

Box 2

Network pattern identification with functional MRI

After preprocessing (step **1**), resting-state (rs) functional (f) MRI scans from healthy control individuals and patients with a disease (here Parkinson disease (PD)) are transformed into a single voxel-by-time series matrix (step **2**), which is analysed with spatial group independent component analysis (ICA)[206] to generate group-wise independent component (IC) maps (step **3**). For convenience, only subjects 1 and *i* are shown but in practice scans from many patients and control individuals would be analysed. Bootstrap resampling is performed to assess the reliability of the group-wise ICs. To obtain ICA spatial maps for the imaging data, dual regression is applied to estimate the time courses and spatial maps for each individual (step **4**). A subject score is computed for each IC in the rs-fMRI data from every individual in the network identification group. These values, which represent the expression of a particular IC in the individual's scan, are computed as the dot product of the corresponding individual and group spatial maps (step **5**). All ICs are then entered into a logistic regression model with bootstrap resampling to identify the subset of ICs that best separate patients and control individuals (step **6**). A histogram ranked in order of descending frequency displays the relative contribution of each IC to the logistic model. Inflection points within the discretized curve are used to identify the most relevant ICs for pattern generation. The corresponding subject scores for these ICs are entered into a second set of logistic models, and bootstrap resampling is again used to estimate the corresponding regression weights (coefficients) for each of the selected ICs (step **7**). Expression levels for the fMRI-based PD-related pattern (fPDRP)[55] are computed as a linear combination of the subject scores for each of the selected ICs weighted by the corresponding regression coefficients.

The fPDRP can be applied to rs-fMRI scan data from prospectively identified individual patients. Dual regression is used to estimate spatial maps for each patient using the group IC maps identified in the pattern derivation procedure. Subject scores for the fPDRP are computed by linear combination of expression levels for the selected ICs, using the coefficients computed in the derivation step.

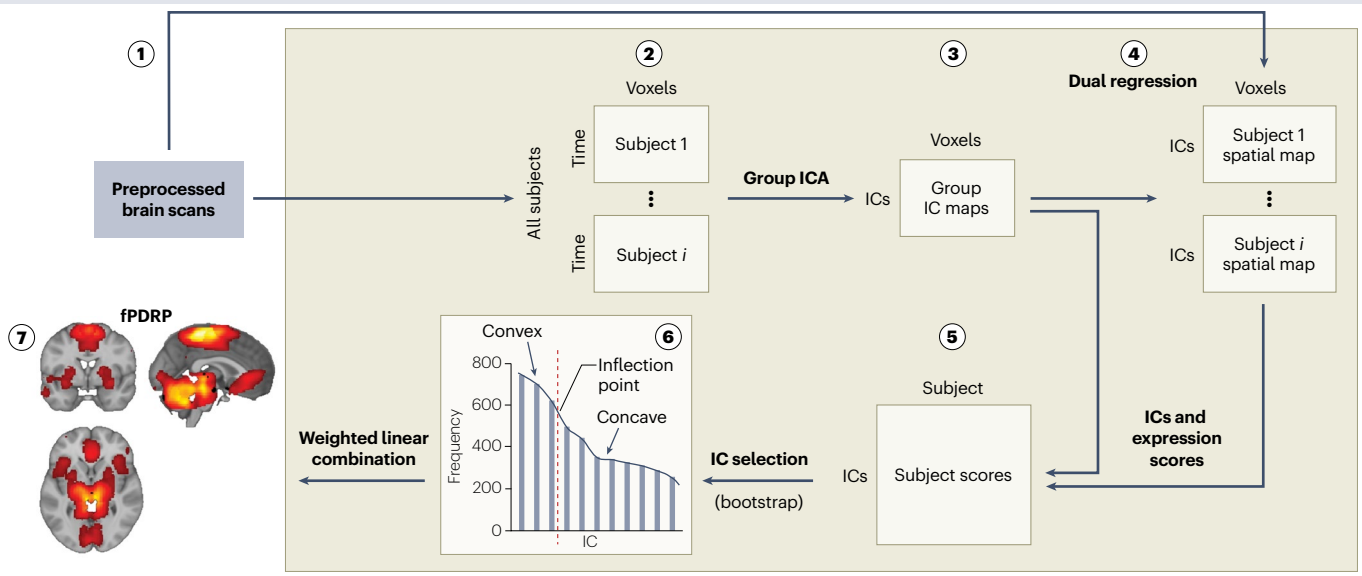

functional topographies as well as their relative contributions to overall network activity. That said, the region-to-region connections (or 'edges') that define the internal structure of a network are equally important, particularly in studies of functional adaptations to underlying neurodegenerative pathology. Graph theory, a discrete branch of mathematics, offers a valuable way to describe changes in functional architecture by delineating the specific regions and connections that form the disease network[60]. Nodes can be defined in various ways, ranging from individual voxels or clusters to anatomically defined regions of interest based on standardized cytoarchitectonic atlases. Connections between nodes are typically defined by distance metrics, among which correlations and partial correlations are most commonly used[61]. Computational algorithms based on graph theory have also been used to isolate small communities of connected regions (termed modules or subgraphs) within the overall network space[62,63]. Connectivity patterns in different groups of individuals, at different time points and under various treatment conditions can be assessed by rigorously computing relevant graph metrics either for validated disease networks as a whole or for key subgraphs[64–67].

Connectivity in graphs can be explored on a local or global level. On a local level, the simplest connectivity measure is nodal degree centrality, which is determined by the number of connections an individual node has with other nodes. By contrast, global metrics can be used to describe connectivity patterns for the network as a whole, which in turn influence information flow through the graph[68]. In this regard, network properties such as characteristic path length, clustering coefficient, small-worldness, modularity and assortativity can be used to recognize network-wide connectivity patterns related to disease state and treatment condition. Indeed, at the module level, these measures might help to distinguish between adaptive and pathological connectivity changes within disease networks[69–71].

Motor-related neurodegeneration

Parkinson disease and related disorders

PD is pathologically characterized by Lewy body formation and deposition of α-synuclein aggregates in the brain, which begins in the lower brainstem and olfactory system, spreads into the midbrain with involvement of the substantia nigra pars compacta and culminates in neurodegeneration in neocortical regions[72,73]. The clinical features of PD tend to correlate with the progression of these pathological changes and with alterations in functional network activity. For example, loss of dopaminergic neurons in the substantia nigra causes dysregulation of a set of cortico-basal ganglia-thalamo-cortical motor circuits that results in emergence of the cardinal symptoms of the disorder — bradykinesia, rigidity and tremor[74]. Although clinical progression of PD generally parallels the stereotyped sequence of pathological changes described above, exceptions have been noted, such as the appearance of subtle cognitive changes before the onset of motor symptoms. Dysfunction of brainstem and basal forebrain neurotransmitter pathways that involve monoaminergic and cholinergic nuclei are likely to occur early in the disease course, long before α-synuclein deposition in the cerebral cortex. In any event, most patients with PD will develop measurable cognitive deficits during the course of the disease[75]. Indeed, both the motor and cognitive clinical manifestations of PD are linked to characteristic brain networks through which focal areas of neurodegeneration affect the function of downstream regions in a disease-specific manner[16,76,77].

Several pathologically distinct neurodegenerative disorders also present with parkinsonism but typically have a worse prognosis than idiopathic PD and do not respond to the pharmacological and surgical interventions used to treat this disorder. Atypical parkinsonian syndromes (APSs), which include multiple system atrophy (MSA), progressive supranuclear palsy (PSP) and cortico-basal degeneration (CBD), can be difficult to differentiate from PD, particularly in the early clinical stages of these diseases[78]. Despite the similarity of their clinical features, the sequence of spread of pathological changes in APSs differs from that in PD, as do the network topographies associated with these diseases[79–82]. Multivariate approaches involving functional brain imaging data enable the identification of disease-specific networks that can be used to evaluate and distinguish between these disorders.

Parkinson disease motor network. A PD-related pattern (PDRP) identified using FDG PET and SSM–PCA has been extensively validated in more than a dozen cohorts of patients and healthy individuals worldwide. Originally identified in a North American population[83], the PDRP was subsequently replicated in independent cohorts of patients with PD in Europe, Asia and the USA[70,84–88]. PDRP topography is characterized by increased glucose metabolism in the putamen, pallidum, thalamus, pons and cerebellum, with relative reductions in glucose metabolism in the premotor and posterior parietal areas. Expression levels for this pattern in patients with PD are consistently correlated with the severity of bradykinesia and rigidity[29,36,55,84,86] and reflect changes in cortico-striato-pallido-thalamo-cortical motor circuits[76,89]. Additional circuits are involved in parkinsonian tremor, related to increased expression of a separate network representing the cerebello-thalamo-cortical motor circuit[36,90,91]. PDRP topographies identified at various research centres in independent populations of patients scanned using different tomographs are remarkably similar despite differences in instrumentation and scanning procedures[70,86,92] and their respective expression levels are closely correlated at the individual patient level[70,84]. Although the PDRP was originally identified in patients with PD of mild to moderate severity who had previously begun daily treatment with dopaminergic drugs[16,83], the same pattern was also identified in drug-naive patients[70].

Of note, when measured hemisphere by hemisphere, PDRP expression levels were elevated to a similar degree both ipsilateral and contralateral to the most-affected body side in patients with unilateral (hemi) PD as well as in those with bilateral limb involvement[93]. This symmetry of PDRP expression contrasts with the asymmetries in clinical features and nigrostriatal dopaminergic dysfunction that characterize idiopathic PD and suggests that these measures capture different aspects of the underlying disease process[93]. Unfortunately, in the absence of data from (rare) patients with asymmetrical presentations of MSA or PSP, it is not clear whether symmetrical brain network abnormalities also occur in this context.

Although an algorithm to characterize these disease networks using rs-fMRI was developed only 5 years ago[55], the resulting fMRI-based PD-related pattern (fPDRP) has already been independently validated[56]. fPDRP networks identified in two independent patient populations were topographically similar[56], and the original FDG PET-based PDRP and fPDRP expression levels correlated closely in patients scanned with both imaging modalities[55]. Abnormally elevated expression levels for FDG PET PDRP were observed in perfusion scans from patients with PD acquired with $H_2{}^{15}O$ PET[83] or ASL MRI[94,95]. SSM–PCA has also been used to identify PDRP-like topographies in structural MRI[96] and ASL MRI[97,98] scans from patients with PD and healthy individuals. Although some aspects of these topographies were shared with the FDG PET PDRP, discrimination of patients with PD from healthy individuals was less accurate with either of these two imaging modalities than with FDG PET. This discrepancy might be attributable to the increased variability of regional cerebral blood flow measurements compared with

glucose metabolism and the limited sensitivity of structural MRI to subtle volumetric changes such as those typically seen in PD. Moreover, many of the patients with PD in these studies were receiving levodopa or carbidopa treatment, which, by uncoupling cerebral blood flow from metabolic activity in key PDRP regions, might confound network measurements obtained during perfusion scans[24,25].

New analytical techniques based on graph theory have provided insights into the organization of brain networks in health and disease[99]. Visualization of the structure of complex networks has been achieved by mapping the sensitivity of nodal centrality measures to changes in incident connections[100]. Our own studies using this approach showed that the PDRP comprised two distinct subnetworks: a core zone, composed of a set of metabolically active and tightly interconnected nodes located in the putamen, globus pallidus and thalamus; and a peripheral zone, composed of less metabolically active and relatively loosely connected cortical nodes[69]. In subsequent studies, we substantiated this core–periphery structure of the PDRP using conventional community detection methods[101]. In this regard, graph analysis revealed distinct connectivity patterns in these two PDRP modules, along with abnormal information flow through the PDRP network in patients with PD[69,71,101]. The presence of differing network connectivity patterns in two subgroups of patients with genotypes associated with either slowly progressing or rapidly progressing PD[102,103] suggests that disease networks such as the PDRP exist in different configurations depending on the disease duration and the degree of functional adaptation that has taken place[71].

Parkinson disease cognition network. Cognitive impairment in individuals with PD is linked to the disruption of normal resting-state networks (particularly the default mode network (DMN))[104–106] and increased expression of an abnormal PD-related cognition network associated with impaired memory and executive dysfunction[107–109]. Cognitive dysfunction in patients with PD is thought to involve multiple inter-related mechanisms, including degeneration of ascending dopaminergic and cholinergic pathways and progressive Lewy body pathology in the limbic and neocortical regions. How these changes affect the function of normal and disease-related brain networks is a topic of ongoing investigation[110,111].

The PD cognition-related pattern (PDCP) was originally identified in FDG PET data from patients with PD without dementia who had a range of neuropsychological performance scores[107,112] and was subsequently validated in four independent cohorts of patients[109,113,114]. The rs-fMRI-based fPDCP was subsequently identified and validated using a modified ICA algorithm[55], and a detailed study of its topography has been published[110]. Analysis of FDG PET scans from 153 patients with PD who underwent neuropsychological evaluation at the time of imaging revealed a strong inverse correlation between increasing PDCP expression levels and loss of normal DMN activity[105,110]. Although the PDCP and DMN share approximately 50% of their regional variance, these two networks were not interchangeable. In fact, our group found that fPDCP topography in patients with PD reflected loss of the ventral component of the DMN (corresponding to the posterior cingulate region and precuneus), whereas the anterior and posterior components of the DMN remained intact in these individuals. Apart from loss of the ventral DMN, the fPDCP included contributions from other brain regions, such as the medial temporal and lateral fronto-parietal regions[110]. Of note, the PDRP and PDCP networks are topographically unrelated.

The DMN has been implicated in cognitive functions involved in memory and abstract reasoning, as well as other domains[115]. Although disruption of DMN structure and function has been observed in patients with PD or Alzheimer disease[105,110], the contribution of this network to neurodegenerative diseases and correlation of DMN changes with neuropsychological test performance is beyond the scope of this Review.

Network changes during disease progression and treatment. Idiopathic rapid eye movement (REM) sleep behaviour disorder (RBD) is a prodromal syndrome that can evolve into clinical α-synucleinopathy-related syndromes, including idiopathic PD, DLB and MSA[116,117]. Indeed, PDRP expression levels were elevated in several independent groups of individuals with idiopathic RBD, to levels between those of healthy individuals and those of patients with early-stage idiopathic PD[118–120]. Moreover, two clinical follow-up studies suggest that individuals with idiopathic RBD who subsequently develop PD or DLB have demonstrable elevations in PDRP expression levels at baseline[118,119]. Limited data suggest that individuals with idiopathic RBD and subnormal PDRP expression are more likely to develop MSA than they are to develop idiopathic PD or DLB[118], although this suggestion remains to be confirmed. Another group of researchers argued that a metabolic covariance pattern, termed PDRBD-RP, which was identified in patients with new-onset PD who had premorbid RBD, was a better predictor of phenotypic conversion to PD than was the standard PDRP[121]. Of note, the PDRBD-RP and PDRP differed primarily in the premotor cortex, which contributed more to PDRBD-RP topography than to the PDRP.

In this regard, idiopathic RBD-related covariance patterns have been identified in FDG PET scans from individuals with idiopathic RBD who have no clinical evidence of PD[120,122–124]. Overall, these patterns were similar to the original PDRP but show increased topographic variation across cohorts. This heterogeneity might stem from low levels of PDRP expression present at preclinical disease stages, or alternatively from differences in the proportions of included individuals at each centre who went on to develop PD, DLB or MSA. Large longitudinal studies of individuals with RBD who go on to develop PD or other α-synucleinopathies will be needed to assess the value of the respective metabolic covariance patterns (singly or in combination) as predictors of phenotypic conversion. Although conclusive differential diagnostic data are currently unavailable, ongoing longitudinal studies in RBD cohorts will help to determine which network most accurately predicts phenotypic conversion in these individuals.

Multiple studies have demonstrated linear progression of PDRP expression with advancing disease[39,93,125,126]. By the same token, PDCP expression exhibits analogous increases along with cognitive deterioration in patients with PD[93,109,110]. Even so, an analysis of data from multiple imaging centres revealed that expression levels were consistently greater for PDRP than for PDCP when measured in the same patients[82]. This tendency for PDRP predominance has been observed in multiple independent cohorts of patients with PD, suggesting that this network develops earlier in the disease course and progresses more rapidly than the PDCP. Additionally, PDRP predominance is consistent with the Braak sequence of neuropathological changes[73,127] (Fig. 1). In this context, the PDRP can be interpreted as the functional equivalent of Braak stage III–IV pathology[16,33,101] whereas the PDCP can be interpreted as the functional equivalent of Braak stage V[16,109,110] (Fig. 1). However, given the complex interplay of dopaminergic, serotonergic and cholinergic pathways in both PDRP and PDCP spaces, this simplified model of disease progression should be considered hypothetical pending further study. Interestingly, PDRP predominance is not evident in APSs such as MSA and PSP, in which an ascending sequence of pathological spread is not evident[79–81].

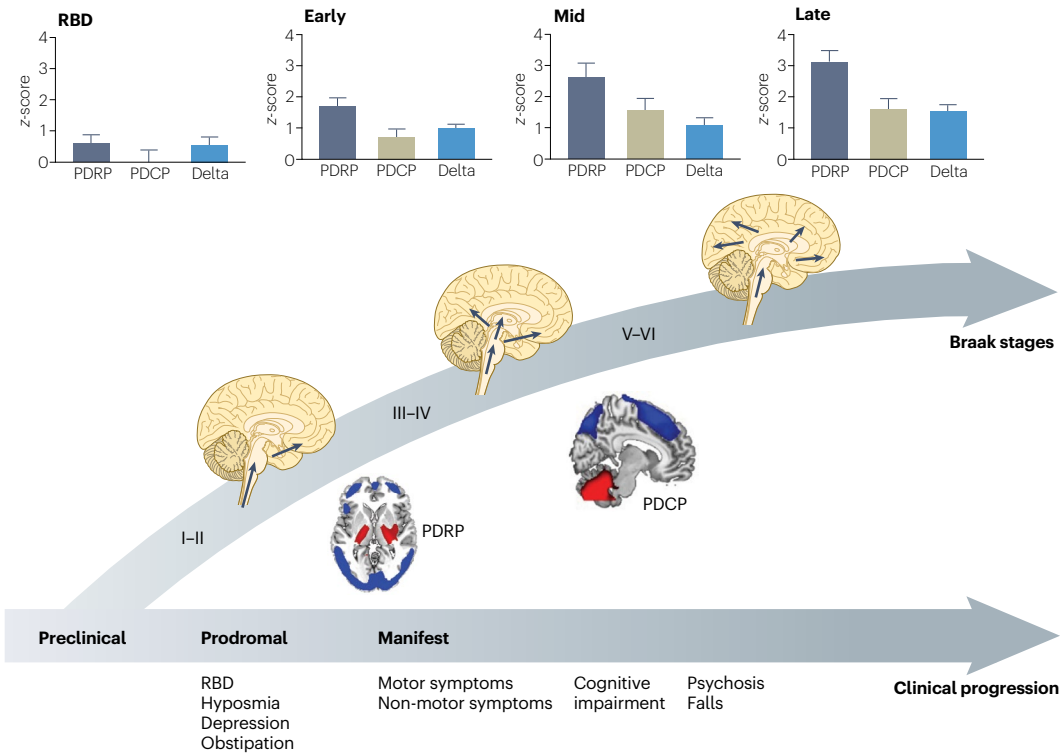

Fig. 1 | Functional brain network alterations associated with Parkinson disease. The Parkinson disease (PD)-related pattern (PDRP) is characterized by network-level functional changes involving the brainstem, basal ganglia and limbic regions, which are the counterpart of Braak stage III–IV pathology[73,127]. The PD cognition-related pattern (PDCP), by contrast, is characterized by functional network changes involving the ventral default mode network and other neocortical regions associated with Braak stage V pathology[110]. The graphs show the stepwise increases in PDRP and PDCP expression levels are seen with disease progression, with PDRP topography appearing earlier than PDCP topography. Interestingly, in individual patients with idiopathic PD, PDRP expression levels are typically greater than the corresponding PDCP values, which results in a positive delta (defined as the difference between PDRP and PDCP expression levels). Delta also increases over time, which is consistent with the stereotypical caudo-rostral sequence of pathological involvement observed in this disorder[82]. Mean PDRP and PDCP expression levels and mean delta values are shown for the prodromal (rapid eye movement (REM) sleep behaviour disorder (RBD)), early (<4 years), middle (4–8 years) and late (>8 years) stages of PD in a cross-sectional sample of 16 patients with RBD and 96 patients with PD.

Symptomatic treatment of PD is associated with reductions in PDRP expression that correlate with clinical outcome[98,128,129]. This effect has been noted in response to acute levodopa administration[55,98,128,130], subthalamic nucleus (STN) deep brain stimulation (DBS)[76,129] and after therapeutic subthalamotomy[131]. Given that PDRP expression levels correlated with spontaneous STN firing rates recorded intra-operatively in patients with PD who were undergoing DBS surgery[89], a decline in PDRP activity (although not in PDCP activity) can be expected following this procedure. Levodopa treatment has complex effects on PDCP and PDRP, as dopamine affects the activity of basal ganglia circuits at multiple levels[132]. For example, PDRP nodes downstream of the striatum in the thalamus, supplementary motor cortex and premotor regions receive dopaminergic input, albeit with reduced terminal density. Levodopa-mediated neurovascular effects might also result in uncoupling of blood flow and metabolism at regional and network levels[24]. Indeed, this phenomenon was found to be particularly striking in patients with PD who experienced drug-induced dyskinesia, a common adverse effect of chronic levodopa therapy[25,133].

Network analysis of functional imaging data is beginning to play an important part in clinical trials in the setting of PD[16,39,134]. In this regard, changes in the expression of well-validated networks such as PDRP and PDCP can be evaluated before and after active treatment or placebo. Indeed, similar approaches can be used for dose-finding and to gauge the effect of treatment on network progression rates. Alternatively, exploratory analyses using supervised PCA techniques, such as OrT–CVA, can be applied to blinded trial data to identify specific treatment-related networks that map the effects of novel interventions on brain pathways. For example, this approach has been used to map the connectivity changes induced by STN adeno-associated virus 2 (AAV2)–*GAD* (encoding glutamate decarboxylase 1) gene therapy in patients with advanced PD[39,135]. Baseline FDG PET scans were obtained from all patients before treatment randomization, as well as during the blinded phase, 6 months and 12 months after either bilateral gene therapy ($n = 16$) or sham surgery ($n = 21$)[135]. Interestingly, PDRP expression increased during the trial period in both groups, indicating the absence of a substantial effect of the treatment on network progression[39]. That said, the effects of gene therapy became apparent at the network level with the use of OrT–CVA and after controlling for the longitudinal changes in PDRP expression. The network changes associated with sham treatment could also be isolated using analogous procedures[136]. Indeed, the resulting network (Fig. 2a), which the researchers termed the AAV2–*GAD*-related pattern (GADRP) exhibited a consistent

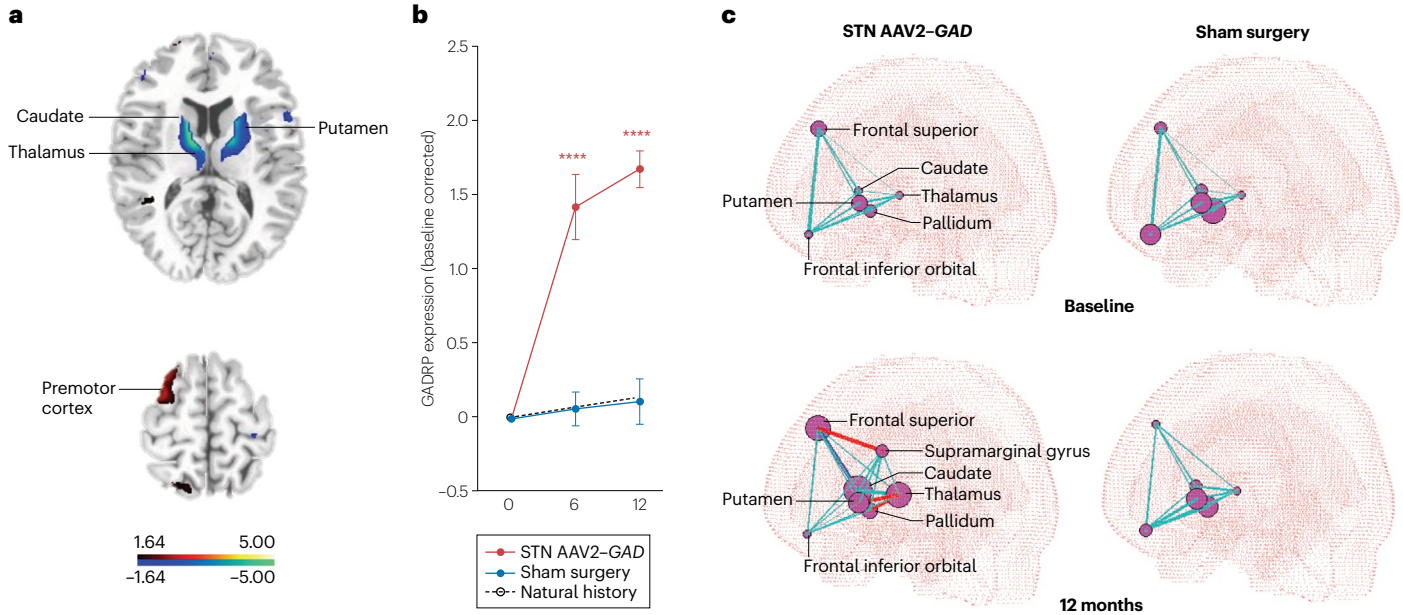

Fig. 2 | Novel functional brain network induced by subthalamic gene therapy for Parkinson disease. a, A metabolic covariance network induced by gene therapy with adeno-associated virus 2 (AAV2)-mediated delivery of *GAD* (encoding glutamate decarboxylase 1) to the subthalamic nucleus (STN) in patients with advanced Parkinson disease (PD). This AAV2–*GAD*-related pattern (GADRP) is characterized by treatment-mediated reductions in activity (blue) in the caudate, putamen, thalamus and inferior frontal gyrus, with relative increases in activity (red) in the parietal lobe and premotor cortex (colour bars: *z* value threshold ±1.64). **b**, Baseline-corrected GADRP expression was measured in a phase II blinded randomized clinical trial that compared AAV2–*GAD* gene therapy with sham surgery[39,135]. Network activity levels increased in the gene therapy group (red line) compared with those in the sham surgery group (blue line) and corresponding values from an independent natural history PD cohort (dashed black line). Changes in unified PD rating scale (UPDRS) values were closely correlated with GADRP expression levels ($P < 0.005$; individual growth model). **c**, Connectivity between GADRP nodes was computed at baseline (top row) and 12 months after intervention (bottom row) in participants who received STN AAV2–*GAD* (left) and those who underwent sham surgery (right). Node-to-node functional interactions were similar at baseline in both groups, whereas a set of new connections was seen at 12 months (bottom row) only after gene therapy. GADRP nodes are represented by spheres with radius proportional to the corresponding nodal connectivity (degree centrality). Connections linking pairs of nodes are represented by cyan lines: values $r \leq 0.5$, fine lines; $r = 0.5–0.6$, medium lines; $r \geq 0.6$, thick lines. Statistically significant positive correlations, bold red lines; statistically significant negative correlations, bold blue lines. For simplicity, only left hemispheres are displayed. Images generated from the authors' own data, published elsewhere[39]. Parts a–c adapted with permission from ref. 39, AAAS.

monotonic increase in expression following gene therapy (Fig. 2b). The changes in GADRP expression levels in these individuals correlated with improvements over time in their performance on standardized motor tests. Graph analysis showed substantial increases in connectivity at key GADRP nodes in the 12 months after gene therapy (Fig. 2c). STN AAV2–*GAD* gene therapy was associated with improvement in abnormal graph metrics such as small-worldness and assortativity that did not occur after sham surgery[39,71]. These changes are consistent with more-efficient information flow through the GADRP network space as the result of gene therapy[39]. Of note, analogous changes in these metrics were also seen in the PDRP space following STN AAV2–*GAD* gene therapy[71], suggesting that appreciable treatment-induced network remodelling can take place even without notable modulation of pattern expression.

A similar approach was used to explore the effects of potentially disease-modifying therapy with nicotinamide riboside, an oral daily supplement that improves mitochondrial respiratory function. FDG PET data were acquired in a blinded 30-day randomized placebo-controlled trial of this treatment in patients with early-stage PD. The analysis revealed the presence of a specific nicotinamide riboside-related pattern (NRRP) in individuals who received the supplement, but not in those who received placebo[40]. The NRRP and PDRP topographies intersected in multiple regions, and treatment-mediated changes in NRRP expression correlated with improved motor ratings under the blind in nicotinamide riboside recipients[40]. Whether this network is a reliable marker of treatment efficacy remains to be determined in future studies.

Effects of genotype. PD is a clinically heterogeneous disorder. Most patients with idiopathic PD have sporadic disease, but a minority carry gene variants associated with this disorder. Indeed, such patients, particularly those with early-stage PD, might be ideal candidates for randomized clinical trials of neuroprotective agents[134,137]. Several imaging studies[138,139] have focused on the functional circuit abnormalities associated with the most common mutations linked to PD: a G>A change at position 6,055 of exon 41 of *LRRK2*, which results in a G2019S amino acid substitution in leucine-rich repeat serine/threonine-protein kinase 2 (LRRK2)[140], and variants in the gene encoding glucosylceramidase (*GBA1*)[102,138]. Patients with PD who carry the *LRRK2*^{G2019S} mutation (PD-LRRK2) typically have lower rates of progression than do individuals with sporadic PD, as well as preserved cognitive function. By contrast,

Glossary

Assortativity
Correlation coefficient between the degree of all nodes on two opposite ends of a link; a measure of the diversity of connections in a graph that provides an index of overall network stability.

Characteristic path length
The average number of edges in the shortest paths connecting the nodes of the network; a measure of the integration of information processing and the global efficiency of the network.

Clustering coefficient
The likelihood that the nearest neighbours of a given network node are themselves connected; an index of the segregation of information processing within the network.

Covariance topographies
Patterns of co-varying regional activity identified by principal component analysis of the individual's scan data.

Degree centrality
The number of connections divided by the number of nodes in the same graph; a measure of the overall connectivity of nodes.

Dimensionality reduction
Mathematical procedures to identify one or more smaller matrices that contain information the same as or similar to the original large data matrix; this approach is used to extract relevant properties of the data (such as specific disease-related topographies) and remove extraneous effects.

Expression levels
Also termed subject scores. The principal component scalar, which quantifies the extent to which a given topographic pattern is represented in a specific individual's scan.

Functional connectivity
Connections between brain regions defined by the magnitude of correlations in spontaneous signal fluctuations (resting-state functional MRI), local metabolic activity ([^{18}F]fluorodeoxyglucose PET), electrical signals (electro-encephalography) or magnetic fields produced by electrical activity (magneto-encephalography).

Functional neuroimaging
Technique to map regional changes in neuronal activity, based typically on blood oxygenation, cerebral metabolism or other physiological signals.

Graph theory
Mathematical approach to studying properties of network structure (nodal organization) and function (information flow).

Modularity
The relationship of the number of edges linking the nodes within a community (module or subgraph) to those linking the different communities for the network as a whole; a means of partitioning the network into organizationally discrete nodal clusters.

Network patterns
Topographical patterns of neural activity in which interconnected brain regions form discrete networks.

Predictive models
Mathematical constructs that predict the likelihood of future events or outcomes based on a set of input data.

Small-worldness
Ratio of clustering coefficient to characteristic path length, normalized to corresponding values from an equivalent random graph; a measure of the balance between segregation and integration of information processing in the network space.

patients with PD who carry *GBA1* variants (PD-GBA) tend to have more aggressive disease and experience more rapid cognitive decline than patients who have sporadic PD[102,141]. Indeed, PDRP and PDCP network expression levels were higher in patients with PD-GBA than in patients with sporadic PD, despite motor symptoms of similar duration and severity[101]. Expression levels for both patterns were lower in patients with PD-LRRK2 than in their counterparts with PD-GBA. Of note, *GBA1* mutation carriers with PD exhibited a larger gap between PDRP and PDCP expression levels than did individuals with sporadic PD. Furthermore, the difference in these values (delta, a potential measure of the transition from motor circuit to cognitive circuit involvement in PD), is greater in *GBA1* mutation carriers and smaller in *LRRK2*^{G2019S} carriers compared with matched patients with sporadic PD[82].

In this vein, graph analysis revealed marked genotypic differences between patients with PD in network structure and information flow in PDRP and PDCP subnetworks[101]. In *LRRK2*^{G2019S} mutation carriers, functional connectivity increased within the metabolically active PDRP core, whereas in *GBA1* mutation carriers, analogous changes were observed in the periphery. These findings and the corresponding graph metrics are consistent with the ascending pattern of pathological changes described above. Analogous genotypic differences between patients with PD were also seen in the PDCP space, with connectivity patterns suggesting a pathological network response in *GBA1* mutation carriers and a stabilizing adaptation in *LRRK2*^{G2019S} mutation carriers[71].

Differential diagnosis of parkinsonism. Network methods can also assist in the differential diagnosis of parkinsonian movement disorders. Parkinsonism can be associated with various neurodegenerative pathologies that are clinically indistinguishable early in the disease course[12,142]. Although specific disease-modification strategies are not currently available for these syndromes, correct diagnosis remains important for several reasons: to confirm a diagnosis of idiopathic PD before surgical intervention such as DBS; to select appropriate participants for clinical trials of new agents or interventions; and for prognostic purposes. In the past 12 years, multivariate analytical approaches have been used alongside disease networks and brain imaging scans to improve diagnostic accuracy in both research and clinical settings[143–146]. For example, a two-step logistic regression algorithm based on PDRP expression levels and disease patterns associated with MSA and PSP (the two most common APSs) has been developed for use in individual patients[145]. The MSA-related pattern (MSARP) is characterized by reduced metabolic activity involving mainly the putamen and cerebellum[147], whereas the PSP-related pattern (PSPRP) is characterized by reduced metabolic activity in the caudate nucleus, premotor and prefrontal cortex, medial thalamus and upper brainstem[147]. The MSARP[148–151] and PSARP[148,150,152,153] have been extensively validated in various populations. Although MSA and PSP can be divided into clinically stereotyped subcategories, expression levels for the corresponding disease patterns tend to be similar in these subcategories, despite substantial differences in phenotype[148,150,152,153]. Of note, a specific covariance pattern has also been isolated for CBD, an uncommon — and, unlike MSA and PSP, which are typically axial and/or symmetrical — clinically highly asymmetrical APS[154], a characteristic that CBD shares with PD[78]. The CBD-related covariance pattern (CBDRP) is characterized by asymmetrical reductions in metabolic activity in the frontal and parietal regions, caudate nucleus and thalamus

that correlate with the observed clinical signs. Thus, as in idiopathic PD, APS-related metabolic topographies are highly reproducible across populations and clinical phenotypes[148–150,152]. Indeed, accurate imaging-based disease classification depends on relative expression levels of the various disease-related patterns, which in turn mirror the underlying pathology[155].

Owing to partial overlap between disease topographies, several networks might be needed to accurately classify individual patients[128]. According to the original three-network diagnostic algorithm[145] (Fig. 3), disease classification based on PDRP, MSARP and PSPRP expression levels is conducted sequentially: the first step discriminates idiopathic PD from APS and the second step discriminates MSA from PSP. This approach has been validated in several groups of patients with parkinsonism who underwent FDG PET to resolve an initially uncertain clinical diagnosis. In these patients, the initial pattern-based classification was compared with the final diagnosis recorded either by a movement disorder specialist several years after imaging[143,146,156] or at autopsy[155]. A meta-analysis showed that the pooled sensitivity of the two-step algorithm was 84% and its pooled specificity was 96%[146], which supports its potential use as a diagnostic test.

Both observer-dependent and observer-independent analytical strategies have been used in conjunction with metabolic imaging to differentiate PD from an APS at the individual patient level. Although observer-dependent strategies such as single-case statistical parametric mapping can be very accurate[157–159], these approaches rely to a certain degree on the training and proficiency of the reader, and the resulting readout is typically binary ('yes' or 'no') in form. By contrast, observer-independent strategies, such as automated pattern-based image classification, can assign a numerical probability to each of the diagnostic alternatives – a useful attribute in the evaluation of individual patients[155].

PDRP and PDCP are perhaps the most thoroughly validated of the known disease networks and provide similar results in FDG PET and rs-fMRI data. Although the MSARP and PSPRP are also validated, less information is available regarding their stability across platforms, particularly in the rs-fMRI setting. Given this limitation, we examined a simple approach in which PDRP and PDCP were used together in a logistic regression model to discriminate individual patients with an APS from those with idiopathic PD. As discussed above, patients with idiopathic PD consistently exhibit PDRP predominance (that is, positive delta values), whereas this characteristic is generally not present in patients with an APS[82]. Indeed, a simple two-network model based on a combination of PDRP and delta (which is mathematically analogous to a combination of PDRP and PDCP) considerably improved the accuracy of the initial clinical judgement of a movement disorder specialist: area under the receiver operator characteristic curve (AUC) 0.85, although categorization was most accurate (AUC 0.95) using the original three-network model[82]. The good accuracy of the two-network method nonetheless renders it a viable alternative to the three-network model, particularly when applied to rs-fMRI data, given the reproducibility of fPDRP and fPDCP on test–retest evaluation[55].

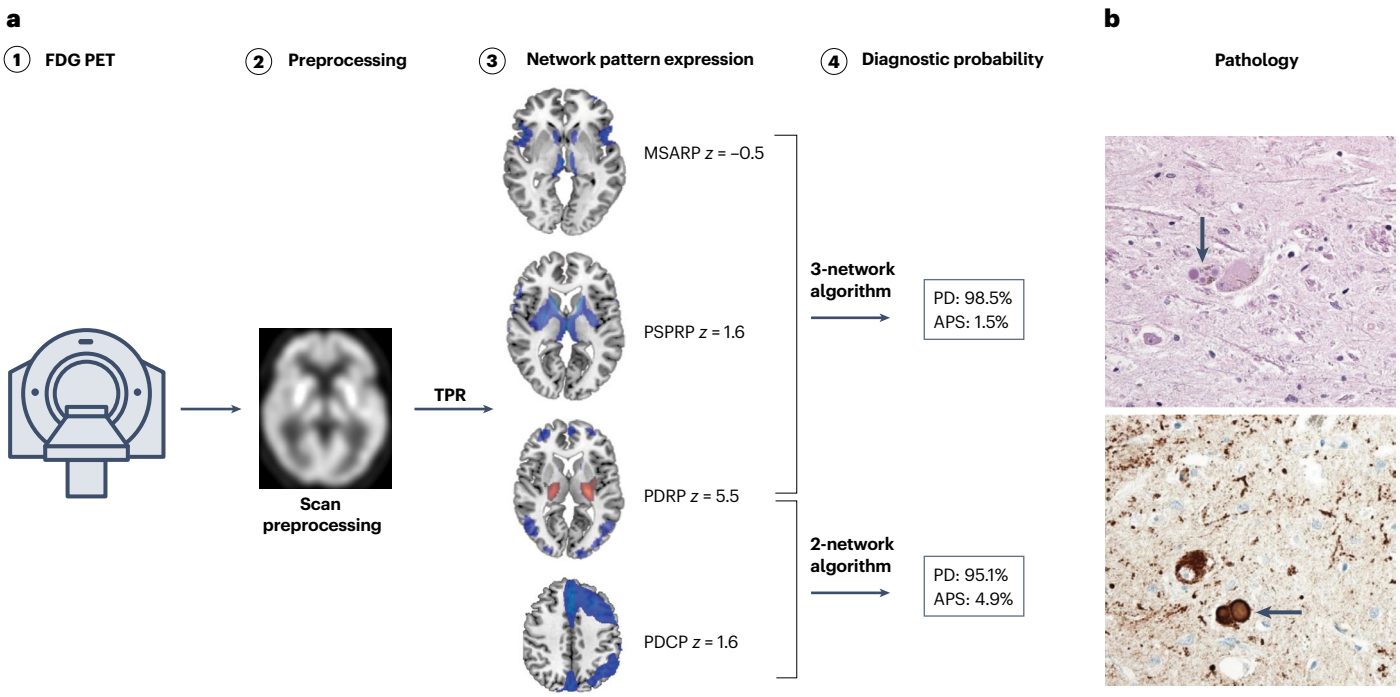

Fig. 3 | Pattern-based classification algorithms for the differential diagnosis of parkinsonism. a, A 52-year-old patient with symmetrical parkinsonism, pronounced axial rigidity, downgaze limitation and poor levodopa response was clinically diagnosed as having an atypical parkinsonian syndrome (APS). He underwent diagnostic [^{18}F]fluorodeoxyglucose (FDG) PET 6 years after disease onset (step **1**). After scan preprocessing (step **2**), expression levels for the multiple system atrophy-related pattern (MSARP), progressive supranuclear palsy-related pattern (PSPRP), Parkinson disease (PD)-related pattern (PDRP) and PD cognition-related pattern (PDCP) networks were calculated using the topographic profile rating (TPR) algorithm (step **3**)[27]. The three-network algorithm, which classified the patient's scan on the basis of PDRP, MSARP and PSPRP expression[145], indicated a higher probability of idiopathic PD than of an APS (step **4**). A simpler two-network algorithm based on PDRP and PDCP expression[82] produced a similar classification result for this individual (step **4**). Post-mortem examination several months after FDG PET revealed characteristic findings of idiopathic PD: top image, severe loss of pigmented neurons in the substantia nigra with reactive gliosis and Lewy bodies in rare preserved neurons (arrow); bottom image, α-synuclein-positive neuronal Lewy bodies (arrow) on immunohistochemical staining[144].

Box 3

The future: machine learning and artificial intelligence

Advances in computer science over the past decade have enabled researchers to explore large imaging datasets in a rapid and efficient manner. Machine learning is a subcategory of artificial intelligence that uses sample data to train predictive models used for classification, regression or pattern recognition[207]. Learning in this context is often unsupervised, meaning that patterns are discovered solely on the basis of unclassified, unlabelled training data. By contrast, learning can also be supervised, which involves continuous updating of the model as more information becomes available. Alternatively, unsupervised learning can be directed towards specific goals by a structured system of rewards and penalties, known as reinforcement learning. For example, the Subtype and Stage Interference (SuStain) machine learning algorithm has been used to resolve temporal and phenotypic heterogeneity in rs-fMRI data and can be used to identify population subgroups that share patterns of disease progression[208]. Similarly, models that can predict cognitive decline have been generated in populations of individuals with autosomal-dominant Alzheimer disease or amyloid-β-positive individuals with MCI using support vector regression. This validated approach uses higher-dimensional projections of the data to predict these individuals' outcomes. Image-based predictive algorithms of this sort can also be used to stratify at-risk individuals for inclusion in therapeutic clinical trials[209]. Although many challenges, such as overfitting, replicability and interpretability remain to be addressed[210], several studies have shown the utility of machine learning and related deep learning algorithms for differential diagnosis and for monitoring disease progression. However, these methods often require large datasets as well as the implementation of effective de-noising algorithms and rigorous harmonization protocols before further analysis, because neuroimaging signals can be noisy and heterogeneous across populations and scanning platforms. Before being considered for routine clinical use, these models must undergo extensive validation in independent datasets obtained in research and clinical settings[211].

Several other approaches used to classify patients with parkinsonian syndromes are based on machine learning algorithms, such as support vector machine, convolutional neural networks[160] and decision trees[161] (Box 3). To date, the accuracy of such classification approaches has been modest, with specificity values ranging from 53% to 76% and sensitivity in the 70–80% range. Classification performance is likely to improve, however, as larger, well-structured imaging datasets become available for training and validation purposes.

Monogenic neurodegenerative disorders

Monogenic neurodegenerative disorders that affect the motor system are rare. These genetically defined disorders, which include Huntington disease and spinocerebellar ataxia, are typically characterized by a fairly consistent phenotype and are gaining research attention because gene-targeted therapies are currently under development[162,163]. Preclinical longitudinal neuroimaging studies offer a window to uncover the brain changes that underlie phenotypic conversion from preclinical or prodromal stages to manifest disease. Indeed, OrT–CVA of longitudinal FDG PET scans from asymptomatic carriers of Huntington disease mutation revealed a metabolic brain network termed the Huntington disease progression pattern (HDPP), for which expression levels increased consistently over 4 years[38]. Of note, high HDPP expression at baseline was associated with early phenotype conversion to manifest Huntington disease in this cohort. The highly statistically significant linear increases in HDPP scores observed in asymptomatic mutation carriers continued through the period of phenotype conversion. This metabolic network might, therefore, be suitable for quantitative assessments of the effect of potential disease-modifying treatments in at-risk individuals.

Spinocerebellar ataxia type 3 (SCA3) is an uncommon monogenic neurodegenerative disorder associated with a covariance pattern that is characterized by reduced metabolic activity in the cerebellum, caudate nucleus and posterior parietal cortex and relatively increased metabolic activity in the somatosensory cortex and limbic system[59]. An rs-fMRI network related to SCA3 (ref. 164) is topographically similar to the original FDG PET[59] pattern and closely correlates with concurrent disease severity ratings.

Cognition-related disorders

Many neurodegenerative diseases present with cognitive decline rather than motor symptoms. Of these, the most common are Alzheimer disease, DLB and FTD[165]. Each of these disorders is associated with characteristic pathological changes, although considerable overlap is evident in the regions involved and in clinical signs and symptoms. Thus, as in parkinsonism, accurate differential diagnosis of these disorders is challenging, particularly for individuals in the early stages of cognitive impairment. Indeed, 25–30% of individuals with neurodegenerative cognitive disorders are misdiagnosed even in speciality clinics[166].

The study of the human connectome and its relationship to underlying brain network abnormalities is essential to the understanding of disease mechanisms and the design of new treatments for these disorders[167]. An emerging body of knowledge describes the normal connectome as well as specific connectivity changes associated with evolving neurodegeneration[168,169]. Detailed characterization of normal cognition-related networks and their changes with advancing age, as well as disease-related connectome alterations, have been used to track the progression of the underlying neurodegenerative process and to predict its spread from one involved layer to the next[170].

Alzheimer disease networks

Alzheimer disease is characterized by abnormal accumulation of amyloid-β (Aβ) in the central hub of the DMN and accumulation of tau protein in the medial temporal lobe[171]. Positivity for Aβ and tau accumulation, which can be currently demonstrated through either cerebrospinal fluid (CSF) analysis or PET imaging (although development of blood biomarkers is rapidly advancing[172]) is necessary for a biological diagnosis of Alzheimer disease[15]. The underlying pathological

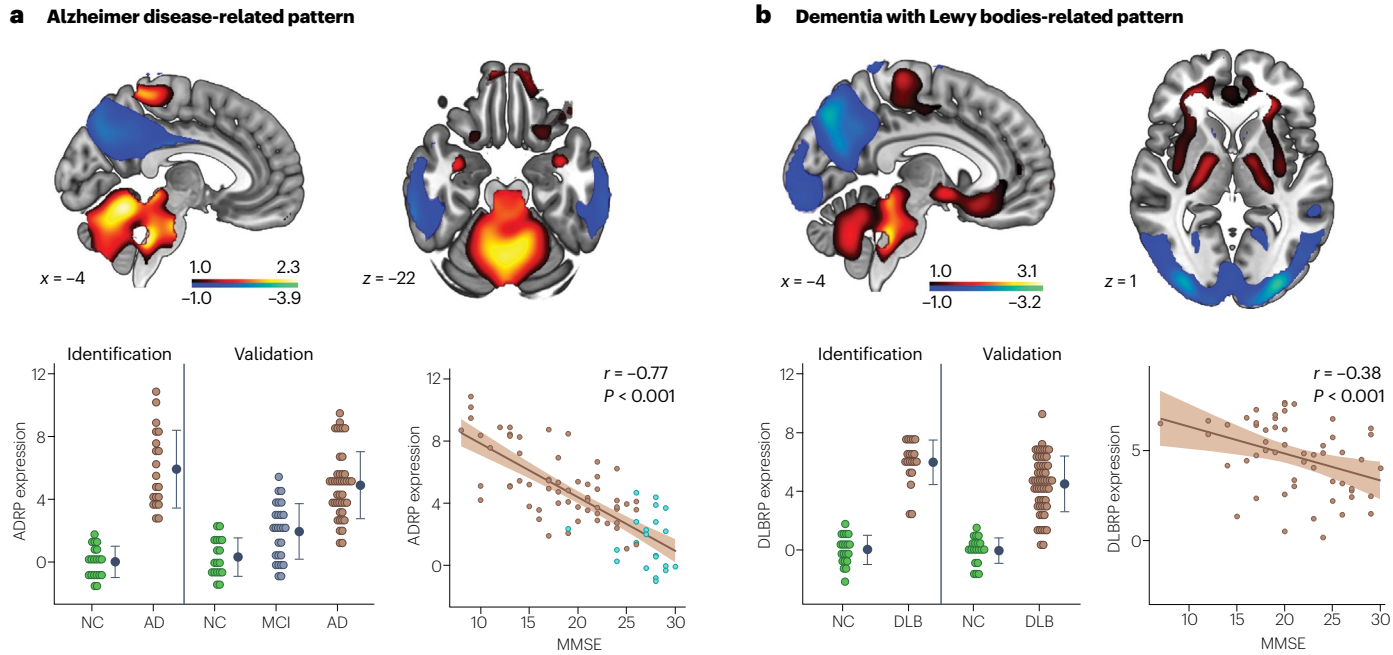

Fig. 4 | Abnormal metabolic covariance patterns associated with Alzheimer disease and dementia with Lewy bodies. a, Top panel: the Alzheimer disease (AD)-related pattern (ADRP) is characterized by reduced metabolic activity (blue) in the precuneus and temporoparietal regions, associated with relative increases (red) in the cerebellum, pons and primary sensorimotor cortex[174]. Bottom panel: ADRP expression levels are elevated in patients with amyloid-β-positive mild cognitive impairment (MCI) and in those with dementia due to AD compared with healthy control individuals (NC)[174]. **b**, Top panel: the dementia with Lewy bodies (DLB)-related metabolic covariance pattern (DLBRP) is characterized by reduced activity (blue) in the precuneus and occipital, inferior parietal and inferior temporal regions, which co-varied with relative increases (red) in the putamen, amygdala, hippocampus, parahippocampal gyrus and cerebellar vermis[192]. Bottom panel: DLBRP expression levels are elevated in patients with DLB compared with those in healthy control individuals. Expression of both ADRP and DLBRP correlates with mini-mental state examination (MMSE) scores[192]. Colour bars: *z* values threshold ±1.0. Graphs and images were generated from the authors' own data, published elsewhere[174,192].

process typically begins years before the appearance of the first clinical symptoms, which range from subjective cognitive decline through mild cognitive impairment (MCI) to dementia[15]. Alzheimer disease pathology has a profound effect on the structural and functional connectomes[167]. Changes are initially seen in DMN function, and these alterations can be accompanied or followed by dysfunction and/or remodelling of connectivity between nodes of the salience and limbic networks[167,173]. Associations between the connectomic changes and underlying pathology have been reviewed at the group level[167]. Analogous relationships with disease-related networks are discussed in the next sections.

The Alzheimer disease-related pattern (ADRP) was originally characterized in cerebral blood flow scans generated with $H_2{}^{15}O$ PET[174], and a relationship between ADRP expression and cognitive decline was demonstrated in a subsequent study[175]. Since then, several similar ADRP topographies have been identified in studies performed at various centres using FDG PET[109,176–178] and dynamic amyloid PET scans[179]. The ADRP is characterized by reduced metabolic activity in the precuneus and temporoparietal regions associated with relative increases in metabolic activity in the cerebellum, pons and primary sensorimotor cortex, which probably reflect the preservation of these regions in the face of neurodegeneration elsewhere (Fig. 4a, top panel). ADRP expression levels were elevated in $A\beta^+$ patients with MCI[178] and patients with MCI who subsequently progressed to dementia[177,180]. Indeed, these values correlated with measures of global cognitive function (Fig. 4a, bottom panel) and with performance on tests of attention, memory, executive function and visuospatial ability[109,176,178]. Although these studies initially identified the ADRP topography in patients with dementia and then applied it prospectively to scans of patients with MCI, a related metabolic pattern was observed when patients with MCI who subsequently developed Alzheimer disease (termed 'converters' in this study) were compared, using SSM–PCA, with matched individuals with MCI who did not develop Alzheimer disease ('non-converters')[181,182]. The resulting Alzheimer disease conversion-related pattern (ADCRP) was similar to previously described ADRP topographies, and ADCRP expression levels also correlated with measures of cognitive dysfunction[181]. That said, ADCRP expression levels were a better predictor of subsequent dementia than clinical and genetic biomarkers[181], the CSF $A\beta_{42}$ to $A\beta_{40}$ ratio[183], regional glucose uptake measures from FDG PET and findings on amyloid PET imaging[184]. The predictive value of ADCRP was also examined in patients with Alzheimer disease-related MCI (individuals who were $A\beta^+$ and tau positive). Expression levels for the ADCRP network were computed in this subgroup and compared with the performance of fluid biomarkers of amyloid accumulation and neurodegeneration. Indeed, ADCRP expression outperformed CSF total tau and plasma neurofilament light chain levels as a predictor of future cognitive decline[185]. Predictions based on ADCRP expression levels were improved by preprocessing to remove non-pathological sources of variability from the scan data[186]. Interestingly, a moderate correlation was observed between ADCRP expression and the Braak stage of neurofibrillary tau

pathology[187]. Also of note is a FDG PET study in which spatial covariance analysis was used to identify a metabolic pattern associated with the risk of AD in a combined group of $A\beta^+$ and $A\beta^-$ healthy individuals[188]. This pattern was characterized by reduced metabolic activity in the precuneus, posterior cingulate cortex, middle temporal and inferior temporal lobes. Expression of this pattern was elevated in the $A\beta^+$ individuals used for pattern identification and for external validation[188]. Moreover, as clinical variants of AD that present with prominent involvement of language, visual perception or executive function display specific patterns of regional hypometabolism[171], it remains to be seen whether or not generic ADRP expression levels in such patients resemble those from patients with typical presentations of Alzheimer disease. Indeed, such variations in clinical symptoms could stem from inter-individual differences in the location and laterality of Alzheimer disease-related cortical changes within the network space[189]. Nonetheless, involvement of posterior midline structures is a consistent feature of the Alzheimer disease network[109,176,178,190,191].

Other dementia networks

Dementia with Lewy bodies. DLB is the next most common neurodegenerative cognitive disorder after Alzheimer disease. DLB is associated with abnormal α-synuclein accumulation in cortical and subcortical brain regions[192] and presents clinically as dementia accompanied by parkinsonism, visual hallucinations, fluctuating cognition and/or RBD[193]. The DLB-related metabolic covariance pattern (DLBRP) is characterized by stereotyped reductions in activity in occipital, inferior parietal and inferior temporal regions and in the precuneus, associated with relative increases in activity in the putamen, amygdala, hippocampus, parahippocampal gyrus and cerebellar vermis (Fig. 4b, top panel). Topographically similar DLBRP networks have been identified in several independent cohorts of patients[194–197]. DLBRP expression levels in these studies correlated either with the individual's cognitive performance at the time of imaging[194,196,197] (Fig. 4b, bottom panel) or with survival duration[196].

DLB shares several clinical and pathological features with Alzheimer disease and PD dementia, and the DLBRP topography

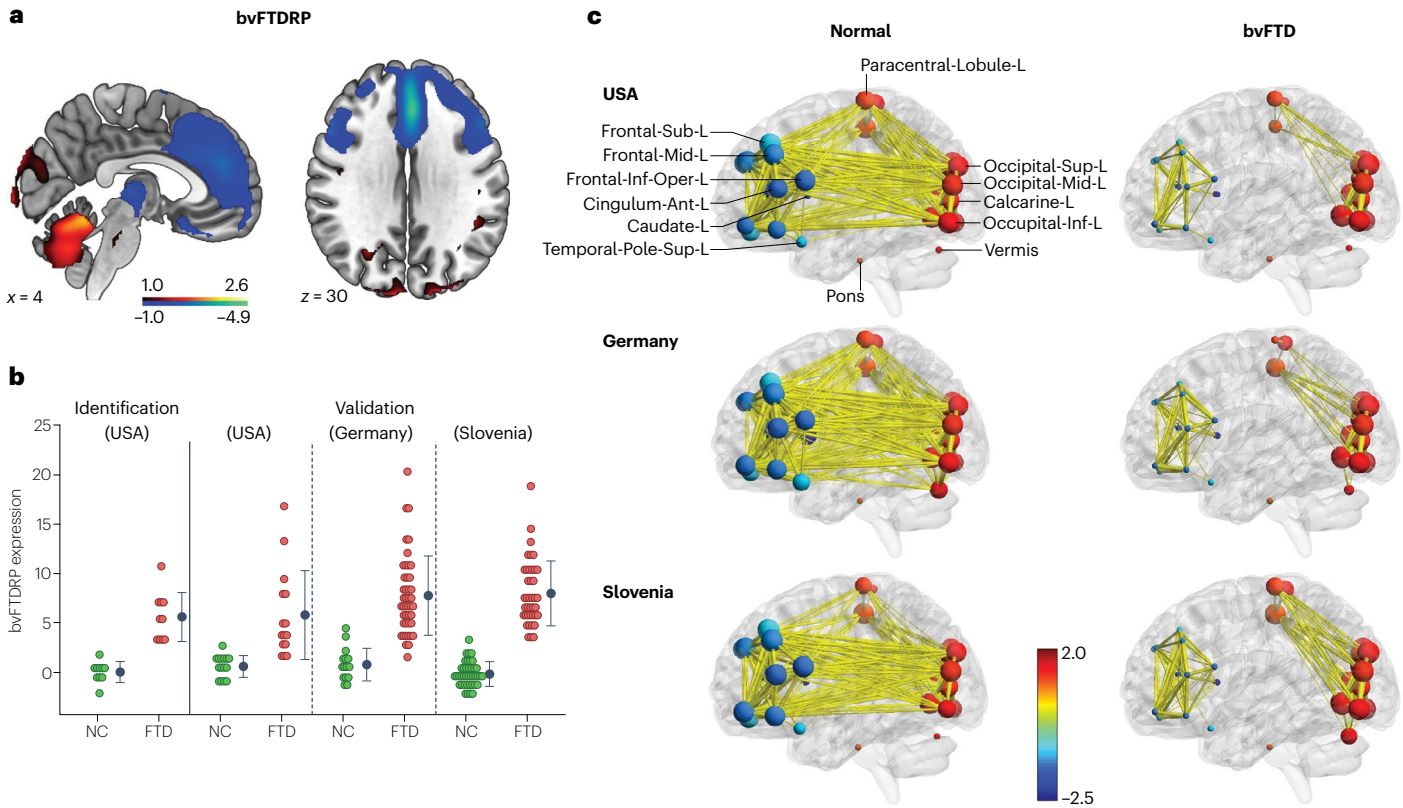

Fig. 5 | Abnormal metabolic covariance pattern associated with frontotemporal dementia. a, The behavioural variant frontotemporal dementia (bvFTD)-related pattern (bvFTDRP) is characterized by reduced activity (blue) in frontotemporal regions, the anterior and middle cingulate gyrus, the insula and thalamus, with relative increases (red) in the occipital lobe and cerebellum. Colour bar: *z* value threshold ±1.0. **b**, Expression levels for this pattern were elevated in patients with bvFTD compared with healthy control individuals (NC) in a derivation sample (USA) used for pattern identification, as well as in independent test samples (USA, Germany and Slovenia) used for validation[203,204]. **c**, Functional connectivity in the network space, viewed from the left, was mapped for scans from patients with bvFTD and healthy control individuals (Normal) in the US, German and Slovenian samples[199,200]. For clarity, only nodes on the left side are labelled; detailed information on all involved nodes is provided elsewhere[204]. Graphical displays revealed similar connectivity patterns in the three locations, with disconnection of the anterior and posterior cortical modules in all patient populations[200]. Edge thickness corresponds to the correlation magnitude. All edges with $r > 0.60$ are presented. bvFTDRP nodes are colour-coded on the basis of the sign of their corresponding region weights; diameter is proportional to corresponding centrality measures. Ant, anterior; frontal-inf-oper, opercular part of inferior frontal gyrus; L, left hemisphere; inf, inferior; sup, superior. Graphs and images were generated from the authors' own data, published elsewhere[199,200]. Part **c** adapted from ref. 200, CC BY 4.0 (https://creativecommons.org/licenses/by/4.0/).

reflects several of these overlapping areas. DLB and idiopathic PD are both Lewy body disorders and more than 85% of patients with DLB also show signs of parkinsonism[198]. In this context, it is perhaps not surprising that the corresponding metabolic topographies are closely related[196,197]. Given that more than 50% of patients with DLB exhibit some Alzheimer disease pathology at post-mortem examination[199], a substantial topographic relationship is expected between DLBRP and ADRP[196]. Conversely, no correlation was discerned between the DLBRP and PDCP topographies or their corresponding expression levels. Indeed, in contrast to PD, in which the extent of cognitive dysfunction correlates with expression of the PDCP[109,110], an analogous relationship with this network was not present in patients with DLB[196].

Of note, multiple studies have reported increased ADRP expression in patients with non-Alzheimer disease dementia[177–179,200]. Indeed, patients with DLB cannot be differentiated from those with Alzheimer disease based solely upon ADRP[177,179,196]. That said, as noted above with regard to pattern-based differentiation of idiopathic PD and APSs, accurate disease classification in a specific individual cannot necessarily be achieved with a single disease-related pattern. Several studies have investigated the use of cross-patterns for differential diagnosis[182]. These topographies are designed to achieve maximal discrimination between two clinically similar disease states, in contrast to generic disease patterns such as ADRP, DLBRP and PDRP, which are each designed to discriminate the corresponding disease state from the normal state. Cross-patterns and other analytical strategies have yielded encouraging results in discriminating patients with DLB from those with Alzheimer disease[194,196,201]. Regardless of the analytical strategy used, DLB was distinguished by relatively preserved activity in the temporal lobes, with either reduced activity in the occipital lobes[194,196] or preserved activity in the precuneus[194,201].

Frontotemporal dementia. The third most common cause of neurodegenerative dementia is FTD. This disorder, in turn, is divided into three clinical subtypes: behavioural variant FTD (bvFTD), non-fluent variant primary progressive aphasia and semantic variant primary progressive aphasia. The most common of these variants is bvFTD, which is associated with changes in personality and behaviour[202]. A bvFTD-related pattern (bvFTDRP) has been identified in three independent populations of patients and healthy control individuals and confirmed in a subgroup with neuropathologically proven bvFTD[203,204]. This metabolic covariance network (Fig. 5a) was characterized by activity reductions in frontal and temporal regions, anterior and middle cingulate gyri, insula and thalamus that were associated with relative activity increases in the occipital cortex and cerebellum. Expression levels of this pattern (Fig. 5b) were consistently higher in patients with bvFTD than in healthy control individuals. Indeed, a closely related bvFTDRP topography was identified in an independent population of patients with autopsy-confirmed bvFTD. Likewise, a strong correlation was observed between expression levels for the two disease patterns in a separate validation cohort[203].

Interestingly, bvFTD topographies were found to overlap with the normal DMN[105], with consistent reductions in expression of the DMN pattern in multiple studies of patients with bvFTD[203–205]. This circumstance suggests that the DMN is an important target of the pathological process that underlies bvFTD. Indeed, visualization of bvFTDRP graphs constructed from three independent patient samples revealed stereotyped changes in the long-range connections that normally link DMN modules[204] (Fig. 5c). Consequently, fragmentation of the DMN is likely to be an important mechanism of cognitive impairment in bvFTD.

Conclusions

The extensive validation of functional brain network topographies across independent clinical centres and imaging platforms and their emerging applications in fMRI, has set the stage for widespread use of this approach in research and clinical decision-making. Increased data sharing and the growing number of open-access databases is likely to accelerate this trend, but will require the development and implementation of rigorous data harmonization procedures. Functional brain network imaging can already facilitate early diagnosis and assist in monitoring disease progression and the effects of treatment in individual patients. As new therapies for neurodegenerative disorders are developed, network biomarkers could narrow the gap between bench and bedside.

Published online: 20 December 2022

References

1. Feigin, V. L. et al. Global, regional, and national burden of neurological disorders, 1990–2016: a systematic analysis for the Global Burden of Disease Study 2016. *Lancet Neurol.* **18**, 459–480 (2019).
2. Vos, T. et al. Global burden of 369 diseases and injuries in 204 countries and territories, 1990–2019: a systematic analysis for the Global Burden of Disease Study 2019. *Lancet,* **396**, 1204–1222 (2020).
3. Nichols, E. et al. Estimation of the global prevalence of dementia in 2019 and forecasted prevalence in 2050: an analysis for the Global Burden of Disease Study 2019. *Lancet Public Health* **7**, e105–e125 (2022).
4. Ou, Z. et al. Global trends in the incidence, prevalence, and years lived with disability of Parkinson's disease in 204 countries/territories from 1990 to 2019. *Front. Public Health* **9**, 776847 (2021).
5. Wanneveich, M., Moisan, F., Jacqmin-Gadda, H., Elbaz, A. & Joly, P. Projections of prevalence, lifetime risk, and life expectancy of Parkinson's disease (2010–2030) in France. *Mov. Disord.* **33**, 1449–1455 (2018).
6. Nichols, E. et al. Global, regional, and national burden of Alzheimer's disease and other dementias, 1990–2016: a systematic analysis for the Global Burden of Disease Study 2016. *Lancet Neurol.* **18**, 88–106 (2019).
7. Dorsey, E. R. et al. Global, regional, and national burden of Parkinson's disease, 1990–2016: a systematic analysis for the Global Burden of Disease Study 2016. *Lancet Neurol.* **17**, 939–953 (2018).
8. Cummings, J., Lee, G., Zhong, K., Fonseca, J. & Taghva, K. Alzheimer's disease drug development pipeline: 2021. *Alzheimers Dement.* **7**, e12179 (2021).
9. McFarthing, K. et al. Parkinson's disease drug therapies in the clinical trial pipeline: 2020. *J. Parkinsons Dis.* **10**, 757–774 (2020).
10. Beach, T. G., Monsell, S. E., Phillips, L. E. & Kukull, W. Accuracy of the clinical diagnosis of Alzheimer disease at National Institute on Aging Alzheimer Disease Centers, 2005–2010. *J. Neuropathol. Exp. Neurol.* **71**, 266–273 (2012).
11. Rizzo, G. et al. Accuracy of clinical diagnosis of dementia with Lewy bodies: a systematic review and meta-analysis. *J. Neurol. Neurosurg. Psychiatry* **89**, 358–366 (2018).
12. Adler, C. H. et al. Low clinical diagnostic accuracy of early vs advanced Parkinson disease: clinicopathologic study. *Neurology* **83**, 406–412 (2014).
13. Joutsa, J., Gardberg, M., Röyttä, M. & Kaasinen, V. Diagnostic accuracy of parkinsonism syndromes by general neurologists. *Parkinsonism Relat. Disord.* **20**, 840–844 (2014).
14. Rizzo, G. et al. Accuracy of clinical diagnosis of Parkinson disease. *Neurology* **86**, 566–576 (2016).
15. Jack, C. R. et al. NIA-AA research framework: toward a biological definition of Alzheimer's disease. *Alzheimers Dement.* **14**, 535–562 (2018).
16. Schindlbeck, K. A. & Eidelberg, D. Network imaging biomarkers: insights and clinical applications in Parkinson's disease. *Lancet Neurol.* **17**, 629–640 (2018).
17. Woo, C. W., Chang, L. J., Lindquist, M. A. & Wager, T. D. Building better biomarkers: brain models in translational neuroimaging. *Nat. Neurosci.* **20**, 365–377 (2017).
This Review provides a valuable summary of multivariate models of brain imaging data as potential biomarkers.
18. Kragel, P. A., Koban, L., Barrett, L. F. & Wager, T. D. Representation, pattern information, and brain signatures: from neurons to neuroimaging. *Neuron* **99**, 257–273 (2018).
19. Peng, S. et al. Dynamic ^{18}F-FPCIT PET: quantification of Parkinson disease metabolic networks and nigrostriatal dopaminergic dysfunction in a single imaging session. *J. Nucl. Med.* **62**, 1775–1782 (2021).
20. Christie, I. N., Wells, J. A., Kasparov, S., Gourine, A. V. & Lythgoe, M. F. Volumetric spatial correlations of neurovascular coupling studied using single pulse opto-fMRI. *Sci. Rep.* **7**, 41583 (2017).
21. Agarwal, S., Sair, H. I., Yahyavi-Firouz-Abadi, N., Airan, R. & Pillai, J. J. Neurovascular uncoupling in resting state fMRI demonstrated in patients with primary brain gliomas. *J. Magn. Reson. Imaging* **43**, 620–626 (2016).
22. Chen, J., Venkat, P., Zacharek, A. & Chopp, M. Neurorestorative therapy for stroke. *Front. Hum. Neurosci.* **8**, 382 (2014).

23. Østergaard, L. et al. Capillary transit time heterogeneity and flow-metabolism coupling after traumatic brain injury. *J. Cereb. Blood Flow. Metab.* **34**, 1585–1598 (2014).
24. Hirano, S. et al. Dissociation of metabolic and neurovascular responses to levodopa in the treatment of Parkinson's disease. *J. Neurosci.* **28**, 4201–4209 (2008).
25. Jourdain, V. A. et al. Flow-metabolism dissociation in the pathogenesis of levodopa-induced dyskinesia. *JCI Insight* **1**, e86615 (2016).
26. Guedj, E. et al. EANM procedure guidelines for brain PET imaging using ^{18}F FDG, version 3. *Eur. J. Nucl. Med. Mol. Imaging* **49**, 632–651 (2022).
27. Spetsieris, P. G. & Eidelberg, D. Scaled subprofile modeling of resting state imaging data in Parkinson's disease: methodological issues. *Neuroimage* **54**, 2899–2914 (2011).
This paper provides a comprehensive presentation of computational procedures to identify and validate disease-related metabolic covariance patterns.
28. Habeck, C. & Stern, Y. Multivariate data analysis for neuroimaging data: overview and application to Alzheimer's disease. *Cell Biochem. Biophys.* **58**, 53–67 (2010).
An oustanding introduction to the multivariate analyses used to characterize disease-related network topographies.
29. Eidelberg, D. Metabolic brain networks in neurodegenerative disorders: a functional imaging approach. *Trends Neurosci.* **32**, 548–557 (2009).
30. Alexander, G. E. & Moeller, J. R. Application of the scaled subprofile model to functional imaging in neuropsychiatric disorders: a principal component approach to modeling brain function in disease. *Hum. Brain Mapp.* **2**, 79–94 (1994).
31. Sala, A. & Perani, D. Brain molecular connectivity in neurodegenerative diseases: recent advances and new perspectives using positron emission tomography. *Front. Neurosci.* **13**, 617 (2019).
32. Yakushev, I., Drzezga, A. & Habeck, C. Metabolic connectivity: methods and applications. *Curr. Opin. Neurol.* **30**, 677–685 (2017).
33. Spetsieris, P. G. & Eidelberg, D. Spectral guided sparse inverse covariance estimation of metabolic networks in Parkinson's disease. *Neuroimage* **226**, 117568 (2021).
This paper facilitates the biological interpretion of disease networks by visualizing relevant node-to-node connections using graphical displays.
34. Jollife, I. T. & Cadima, J. Principal component analysis: a review and recent developments. *Philos. Trans. R. Soc. A Math. Phys. Eng. Sci.* **374**, 20150202 (2016).
35. Habeck, C. et al. A new approach to spatial covariance modeling of functional brain imaging data: ordinal trend analysis. *Neural Comput.* **17**, 1602–1645 (2005).
36. Mure, H. et al. Parkinson's disease tremor-related metabolic network: characterization, progression, and treatment effects. *Neuroimage* **54**, 1244–1253 (2011).
37. Mure, H. et al. Improved sequence learning with subthalamic nucleus deep brain stimulation: evidence for treatment-specific network modulation. *J. Neurosci.* **32**, 2804–2813 (2012).
38. Tang, C. C. et al. Metabolic network as a progression biomarker of premanifest Huntington's disease. *J. Clin. Invest.* **123**, 4076–4088 (2013).
39. Niethammer, M. et al. Gene therapy reduces Parkinson's disease symptoms by reorganizing functional brain connectivity. *Sci. Transl. Med.* **10**, eaau0713 (2018).
A study that shows how subthalamic gene therapy for advanced PD induces a unique and more-efficient metabolic network that correlates with treatment outcome.
40. Brakedal, B. et al. The NADPARK study: a randomized phase I trial of nicotinamide riboside supplementation in Parkinson's disease. *Cell Metab.* **34**, 396–407 (2022).
This study uses similar methods to those in the preceding paper to identify a treatment-related network induced by a supplement that boosts mitochondrial respiration in early PD.
41. Li, B. & Freeman, R. D. Neurometabolic coupling between neural activity, glucose, and lactate in activated visual cortex. *J. Neurochem.* **135**, 742–754 (2015).
42. Stoessl, A. J. Glucose utilization: still in the synapse. *Nat. Neurosci.* **20**, 382–384 (2017).
43. Patel, A. B. et al. Direct evidence for activity-dependent glucose phosphorylation in neurons with implications for the astrocyte-to-neuron lactate shuttle. *Proc. Natl Acad. Sci. USA* **111**, 5385–5390 (2014).
44. Xiang, X. et al. Microglial activation states drive glucose uptake and FDG-PET alterations in neurodegenerative diseases. *Sci. Transl. Med.* **13**, eabe5640 (2021).
45. Savio, A. et al. Resting-state networks as simultaneously measured with functional MRI and PET. *J. Nucl. Med.* **58**, 1314–1317 (2017).
46. Marchitelli, R. et al. Simultaneous resting-state FDG-PET/fMRI in Alzheimer disease: relationship between glucose metabolism and intrinsic activity. *Neuroimage* **176**, 246–258 (2018).
47. Jamadar, S. D. et al. Metabolic and hemodynamic resting-state connectivity of the human brain: a high-temporal resolution simultaneous BOLD-fMRI and FDG-fPET multimodality study. *Cereb. Cortex* **31**, 2855–2867 (2021).
48. Sala, A., Lizarraga, A., Ripp, I., Cumming, P. & Yakushev, I. Static versus functional PET: making sense of metabolic connectivity. *Cereb. Cortex* **32**, 1125–1129 (2021).
49. Watabe, T. & Hatazawa, J. Evaluation of functional connectivity in the brain using positron emission tomography: a mini-review. *Front. Neurosci.* **13**, 775 (2019).
50. Cao, J. & Worsley, K. The geometry of correlation fields with an application to functional connectivity of the brain. *Ann. Appl. Probab.* **9**, 1021–1057 (1999).
51. Sun, F. T., Miller, L. M. & D'Esposito, M. Measuring interregional functional connectivity using coherence and partial coherence analyses of fMRI data. *Neuroimage* **21**, 647–658 (2004).
52. Hyvärinen, A. Independent component analysis: recent advances. *Philos. Trans. R. Soc. A Math. Phys. Eng. Sci.* **371**, 20110534 (2013).
53. Baggio, H.-C. et al. Cognitive impairment and resting-state network connectivity in Parkinson's disease. *Hum. Brain Mapp.* **36**, 199–212 (2015).
54. Calhoun, V. D., Liu, J. & Adalı, T. A review of group ICA for fMRI data and ICA for joint inference of imaging, genetic, and ERP data. *Neuroimage* **45**, S163–S172 (2009).
55. Vo, A. et al. Parkinson's disease-related network topographies characterized with resting state functional MRI. *Hum. Brain Mapp.* **38**, 617–630 (2017).
This study shows how rs-fMRI can be used to identify disease-related topographies that are similar to their PET counterparts.
56. Rommal, A. et al. Parkinson's disease-related pattern (PDRP) identified using resting-state functional MRI: validation study. *Neuroimage Rep.* **1**, 100026 (2021).
57. Greuel, A. et al. GBA variants in Parkinson's disease: clinical, metabolomic, and multimodal neuroimaging phenotypes. *Mov. Disord.* **35**, 2201–2210 (2020).
58. Steidel, K. et al. Dopaminergic pathways and resting-state functional connectivity in Parkinson's disease with freezing of gait. *Neuroimage Clin.* **32**, 102899 (2021).
59. Meles, S. K. et al. The cerebral metabolic topography of spinocerebellar ataxia type 3. *Neuroimage Clin.* **19**, 90–97 (2018).
60. Sporns, O. Graph theory methods: applications in brain networks. *Dialogues Clin. Neurosci.* **20**, 111–121 (2018).
Overview of graph theory as applied to the study of brain networks.
61. Muskulus, M., Houweling, S., Verduyn-Lunel, S. & Daffertshofer, A. Functional similarities and distance properties. *J. Neurosci. Methods* **183**, 31–41 (2009).
62. Newman, M. *Networks* (Oxford Univ. Press, 2010).
63. Fortunato, S. Community detection in graphs. *Phys. Rep.* **486**, 75–174 (2010).
64. Agosta, F. et al. Brain network connectivity assessed using graph theory in frontotemporal dementia. *Neurology* **81**, 134–143 (2013).
65. Imai, M. et al. Metabolic network topology of Alzheimer's disease and dementia with Lewy bodies generated using fluorodeoxyglucose positron emission tomography. *J. Alzheimers Dis.* **73**, 197–207 (2020).
66. Sala, A. et al. Altered brain metabolic connectivity at multiscale level in early Parkinson's disease. *Sci. Rep.* **7**, 4256 (2017).
67. Yao, Z. et al. A FDG-PET study of metabolic networks in apolipoprotein E ε4 allele carriers. *PLoS ONE* **10**, e0132300 (2015).
68. Sporns, O. & Betzel, R. F. Modular brain networks. *Annu. Rev. Psychol.* **67**, 613–640 (2016).
69. Ko, J. H., Spetsieris, P. G. & Eidelberg, D. Network structure and function in Parkinson's disease. *Cereb. Cortex* **28**, 4121–4135 (2018).
70. Schindlbeck, K. A. et al. Metabolic network abnormalities in drug-naïve Parkinson's disease. *Mov. Disord.* **35**, 587–594 (2020).
71. Vo, A. et al. Adaptive and pathological connectivity responses in Parkinson's disease brain networks. *Cereb. Cortex* https://doi.org/10.1093/cercor/bhac110 (2022).
This study shows that connectivity patterns within the network space distinguish maladaptive changes from beneficial adaptations in PD.
72. Adler, C. H. et al. Unified staging system for Lewy body disorders: clinicopathologic correlations and comparison to Braak staging. *J. Neuropathol. Exp. Neurol.* **78**, 891–899 (2019).
73. Hawkes, C. H., Del Tredici, K. & Braak, H. A timeline for Parkinson's disease. *Parkinsonism Relat. Disord.* **16**, 79–84 (2010).
74. Postuma, R. B. et al. MDS clinical diagnostic criteria for Parkinson's disease. *Mov. Disord.* **30**, 1591–1601 (2015).
75. Aarsland, D. et al. Parkinson disease-associated cognitive impairment. *Nat. Rev. Dis. Prim.* **7**, 47 (2021).
76. Niethammer, M. & Eidelberg, D. Metabolic brain networks in translational neurology: concepts and applications. *Ann. Neurol.* **72**, 635–647 (2012).
77. Meles, S. K., Teune, L. K., de Jong, B. M., Dierckx, R. A. & Leenders, K. L. Metabolic imaging in Parkinson disease. *J. Nucl. Med.* **58**, 23–28 (2017).
78. Stamelou, M. & Bhatia, K. P. Atypical parkinsonism. *Neurol. Clin.* **33**, 39–56 (2015).
79. Kovacs, G. G. et al. Distribution patterns of tau pathology in progressive supranuclear palsy. *Acta Neuropathol.* **140**, 99–119 (2020).
80. Briggs, M. et al. Validation of the new pathology staging system for progressive supranuclear palsy. *Acta Neuropathol.* **141**, 787–789 (2021).
81. Brettschneider, J. et al. Progression of α-synuclein pathology in multiple system atrophy of the cerebellar type. *Neuropathol. Appl. Neurobiol.* **43**, 315–329 (2017).
82. Rus, T. et al. Stereotyped relationship between motor and cognitive metabolic networks in Parkinson's disease. *Mov. Disord.* **37**, 2247–2256 (2022).
83. Ma, Y., Tang, C., Spetsieris, P. G., Dhawan, V. & Eidelberg, D. Abnormal metabolic network activity in Parkinson's disease: test–retest reproducibility. *J. Cereb. Blood Flow. Metab.* **27**, 597–605 (2007).
84. Tomše, P. et al. Abnormal metabolic brain network associated with Parkinson's disease: replication on a new European sample. *Neuroradiology* **59**, 507–515 (2017).
85. Wu, P. et al. Metabolic brain network in the Chinese patients with Parkinson's disease based on ^{18}F-FDG PET imaging. *Parkinsonism Relat. Disord.* **19**, 622–627 (2013).
86. Meles, S. K. et al. Abnormal pattern of brain glucose metabolism in Parkinson's disease: replication in three European cohorts. *Eur. J. Nucl. Med. Mol. Imaging* **47**, 437–450 (2020).
87. Matthews, D. C. et al. FDG PET Parkinson's disease-related pattern as a biomarker for clinical trials in early stage disease. *Neuroimage Clin.* **20**, 572–579 (2018).
88. Teune, L. K. et al. Validation of parkinsonian disease-related metabolic brain patterns. *Mov. Disord.* **28**, 547–551 (2013).
89. Lin, T. P. et al. Metabolic correlates of subthalamic nucleus activity in Parkinson's disease. *Brain* **131**, 1373–1380 (2008).

90. Helmich, R. C., Hallett, M., Deuschl, G., Toni, I. & Bloem, B. R. Cerebral causes and consequences of parkinsonian resting tremor: a tale of two circuits? *Brain* **135**, 3206–3226 (2012).
91. Zach, H. et al. Dopamine-responsive and dopamine-resistant resting tremor in Parkinson disease. *Neurology* **95**, e1461–e1470 (2020).
92. Ko, J. H., Spetsieris, P., Ma, Y., Dhawan, V. & Eidelberg, D. Quantifying significance of topographical similarities of disease-related brain metabolic patterns. *PLoS ONE* **9**, e88119 (2014).
93. Tang, C. C. et al. Hemispheric network expression in Parkinson's disease: relationship to dopaminergic asymmetries. *J. Parkinsons Dis.* **10**, 1737–1749 (2020).
94. Ma, Y. et al. Parkinson's disease spatial covariance pattern: noninvasive quantification with perfusion MRI. *J. Cereb. Blood Flow. Metab.* **30**, 505–509 (2010).
95. Ma, Y. & Eidelberg, D. Functional imaging of cerebral blood flow and glucose metabolism in Parkinson's disease and Huntington's disease. *Mol. Imaging Biol.* **9**, 223–233 (2007).
96. Liu, C. et al. Brain functional and structural signatures in Parkinson's disease. *Front. Aging Neurosci.* **12**, 125 (2020).
97. Melzer, T. R. et al. Arterial spin labelling reveals an abnormal cerebral perfusion pattern in Parkinson's disease. *Brain* **134**, 845–855 (2011).
98. Rane, S. et al. Arterial spin labeling detects perfusion patterns related to motor symptoms in Parkinson's disease. *Parkinsonism Relat. Disord.* **76**, 21–28 (2020).
99. Stam, C. J. Modern network science of neurological disorders. *Nat. Rev. Neurosci.* **15**, 683–695 (2014).
100. Correa, C., Crnovrsanin, T. & Kwan-Liu, M. Visual reasoning about social networks using centrality sensitivity. *IEEE Trans. Vis. Comput. Graph.* **18**, 106–120 (2012).
101. Schindlbeck, K. A. et al. *LRRK2* and *GBA* variants exert distinct influences on parkinson's disease-specific metabolic networks. *Cereb. Cortex* **30**, 2867–2878 (2020).
102. Davis, M. Y. et al. Association of *GBA* mutations and the E326K polymorphism with motor and cognitive progression in Parkinson disease. *JAMA Neurol.* **73**, 1217–1224 (2016).
103. Saunders-Pullman, R. et al. Progression in the *LRRK2*-associated Parkinson disease population. *JAMA Neurol.* **75**, 312–319 (2018).
104. Wolters, A. F. et al. Resting-state fMRI in Parkinson's disease patients with cognitive impairment: a meta-analysis. *Parkinsonism Relat. Disord.* **62**, 16–27 (2019).
105. Spetsieris, P. G. et al. Metabolic resting-state brain networks in health and disease. *Proc. Natl Acad. Sci. USA* **112**, 2563–2568 (2015).
This study identifies the metabolic DMN in healthy individuals and describes the effects of neurodegeneration on expression of this pattern in patients with PD and Alzheimer disease.
106. Ruppert, M. C. et al. The default mode network and cognition in Parkinson's disease: a multimodal resting-state network approach. *Hum. Brain Mapp.* **42**, 2623–2641 (2021).
107. Huang, C. et al. Metabolic brain networks associated with cognitive function in Parkinson's disease. *Neuroimage* **34**, 714–723 (2007).
108. Mattis, P. J., Tang, C. C., Ma, Y., Dhawan, V. & Eidelberg, D. Network correlates of the cognitive response to levodopa in Parkinson disease. *Neurology* **77**, 858–865 (2011).
109. Mattis, P. J. et al. Distinct brain networks underlie cognitive dysfunction in Parkinson and Alzheimer diseases. *Neurology* **87**, 1925–1933 (2016).
110. Schindlbeck, K. A. et al. Cognition-related functional topographies in Parkinson's disease: localized loss of the ventral default mode network. *Cereb. Cortex* **31**, 5139–5150 (2021).
This study uses rs-fMRI to explore the topographic relationship between the PDCP and DMN.
111. Hirano, S. Clinical implications for dopaminergic and functional neuroimage research in cognitive symptoms of Parkinson's disease. *Mol. Med.* **27**, 40 (2021).
112. Huang, C. et al. Metabolic abnormalities associated with mild cognitive impairment in Parkinson disease. *Neurology* **70**, 1470–1477 (2008).
113. Meles, S. K. et al. Abnormal metabolic pattern associated with cognitive impairment in Parkinson's disease: a validation study. *J. Cereb. Blood Flow. Metab.* **35**, 1478–1484 (2015).
114. Trošt, M. et al. Metabolic brain changes related to specific cognitive impairment in non-demented Parkinson's disease patients [abstract #1306]. Presented at 2016 International Congress, International Parkinson and Movement Disorder Society. https://www.mdsabstracts.org/abstract/metabolic-brain-changes-related-to-specific-cognitive-impairment-in-non-demented-parkinsons-disease-patients/ (2016).
115. Smallwood, J. et al. The default mode network in cognition: a topographical perspective. *Nat. Rev. Neurosci.* **22**, 503–513 (2021).
In this paper, the authors attribute the integrative role of the DMN in higher-order cognitive functions to its position at the end of the cortical processing stream.
116. Meles, S. K., et al. in *PET and SPECT in Neurology*. 73–104 (Springer International, 2021).
117. Högl, B., Stefani, A. & Videnovic, A. Idiopathic REM sleep behaviour disorder and neurodegeneration — an update. *Nat. Rev. Neurol.* **14**, 40–56 (2018).
118. Holtbernd, F. et al. Abnormal metabolic network activity in REM sleep behavior disorder. *Neurology* **82**, 620–627 (2014).
119. Kogan, R. V. et al. Four-year follow-up of ^{18}F fluorodeoxyglucose positron emission tomography-based Parkinson's disease-related pattern expression in 20 patients with isolated rapid eye movement sleep behavior disorder shows prodromal progression. *Mov. Disord.* **36**, 230–235 (2021).
120. Ge, J. et al. Assessing cerebral glucose metabolism in patients with idiopathic rapid eye movement sleep behavior disorder. *J. Cereb. Blood Flow. Metab.* **35**, 2062–2069 (2015).
121. Shin, J. H. et al. Parkinson disease-related brain metabolic patterns and neurodegeneration in isolated REM sleep behavior disorder. *Neurology* **97**, e378–e388 (2021).
122. Meles, S. K. et al. The metabolic pattern of idiopathic REM sleep behavior disorder reflects early-stage Parkinson disease. *J. Nucl. Med.* **59**, 1437–1444 (2018).
123. Yoon, E. J. et al. A new metabolic network correlated with olfactory and executive dysfunctions in idiopathic rapid eye movement sleep behavior disorder. *J. Clin. Neurol.* **15**, 175–183 (2019).
124. Wu, P. et al. Consistent abnormalities in metabolic network activity in idiopathic rapid eye movement sleep behaviour disorder. *Brain* **137**, 3122–3128 (2014).
125. Huang, C. et al. Changes in network activity with the progression of Parkinson's disease. *Brain* **130**, 1834–1846 (2007).
126. Tang, C. C., Poston, K. L., Dhawan, V. & Eidelberg, D. Abnormalities in metabolic network activity precede the onset of motor symptoms in Parkinson's disease. *J. Neurosci.* **30**, 1049–1056 (2010).
127. Braak, H. et al. Staging of brain pathology related to sporadic Parkinson's disease. *Neurobiol. Aging* **24**, 197–211 (2003).
128. Ko, J. H., Lerner, R. P. & Eidelberg, D. Effects of levodopa on regional cerebral metabolism and blood flow. *Mov. Disord.* **30**, 54–63 (2015).
129. Ge, J. et al. Metabolic network as an objective biomarker in monitoring deep brain stimulation for Parkinson's disease: a longitudinal study. *EJNMMI Res.* **10**, 131 (2020).
130. Asanuma, K. et al. Network modulation in the treatment of Parkinson's disease. *Brain* **129**, 2667–2678 (2006).
131. Trošt, M. et al. Network modulation by the subthalamic nucleus in the treatment of Parkinson's disease. *Neuroimage* **31**, 301–307 (2006).
132. Rommelfanger, K. S. & Wichmann, T. Extrastriatal dopaminergic circuits of the basal ganglia. *Front. Neuroanat.* **4**, 139 (2010).
133. Jourdain, V. A. et al. Increased putamen hypercapnic vasoreactivity in levodopa-induced dyskinesia. *JCI Insight* **2**, e96411 (2017).
134. Ntetsika, T., Papathoma, P.-E. & Markaki, I. Novel targeted therapies for Parkinson's disease. *Mol. Med.* **27**, 17 (2021).
135. Niethammer, M. et al. Long-term follow-up of a randomized AAV2-*GAD* gene therapy trial for Parkinson's disease. *JCI Insight* **2**, e90133 (2017).
136. Ko, J. H. et al. Network modulation following sham surgery in Parkinson's disease. *J. Clin. Invest.* **124**, 3656–3666 (2014).
This study shows that the clinical response to sham surgery in patients with PD is mediated by a specific metabolic brain network that is active only in patients who are blinded to treatment.
137. Prasuhn, J. & Brüggemann, N. Genotype-driven therapeutic developments in Parkinson's disease. *Mol. Med.* **27**, 42 (2021).
138. Filippi, M., Balestrino, R., Basaia, S. & Agosta, F. Neuroimaging in glucocerebrosidase-associated parkinsonism: a systematic review. *Mov. Disord.* **37**, 1375–1393 (2022).
139. Meles, S. K., Oertel, W. H. & Leenders, K. L. Circuit imaging biomarkers in preclinical and prodromal Parkinson's disease. *Mol. Med.* **27**, 111 (2021).
140. Tolosa, E., Vila, M., Klein, C. & Rascol, O. LRRK2 in Parkinson disease: challenges of clinical trials. *Nat. Rev. Neurol.* **16**, 97–107 (2020).
141. Blauwendraat, C., Nalls, M. A. & Singleton, A. B. The genetic architecture of Parkinson's disease. *Lancet Neurol.* **19**, 170–178 (2020).
142. Beach, T. G. & Adler, C. H. Importance of low diagnostic accuracy for early Parkinson's disease. *Mov. Disord.* **33**, 1551–1554 (2018).
143. Rus, T. et al. Differential diagnosis of parkinsonian syndromes: a comparison of clinical and automated-metabolic brain patterns' based approach. *Eur. J. Nucl. Med. Mol. Imaging* **47**, 2901–2910 (2020).
This study supports the utility of automated pattern-based differential diagnosis of parkinsonism in a real-world clinical setting.
144. Rus, T. et al. Atypical clinical presentation of pathologically proven Parkinson's disease: the role of Parkinson's disease related metabolic pattern. *Parkinsonism Relat. Disord.* **78**, 1–3 (2020).
145. Tang, C. C. et al. Differential diagnosis of parkinsonism: a metabolic imaging study using pattern analysis. *Lancet Neurol.* **9**, 149–158 (2010).
146. Papathoma, P. E. et al. A replication study, systematic review and meta-analysis of automated image-based diagnosis in parkinsonism. *Sci. Rep.* **12**, 2763 (2022).
147. Eckert, T. et al. Abnormal metabolic networks in atypical parkinsonism. *Mov. Disord.* **23**, 727–733 (2008).
148. Ge, J. et al. Reproducible network and regional topographies of abnormal glucose metabolism associated with progressive supranuclear palsy: multivariate and univariate analyses in American and Chinese patient cohorts. *Hum. Brain Mapp.* **39**, 2842–2858 (2018).
149. Shen, B. et al. Reproducible metabolic topographies associated with multiple system atrophy: network and regional analyses in Chinese and American patient cohorts. *Neuroimage Clin.* **28**, 102416 (2020).
150. Tomše, P. et al. Abnormal metabolic covariance patterns associated with multiple system atrophy and progressive supranuclear palsy. *Phys. Med.* **98**, 131–138 (2022).

151. Poston, K. L. et al. Network correlates of disease severity in multiple system atrophy. *Neurology* **78**, 1237–1244 (2012).
152. Martí-Andrés, G. et al. Multicenter validation of metabolic abnormalities related to PSP according to the MDS-PSP criteria. *Mov. Disord.* **35**, 2009–2018 (2020).
This study shows the robustness and reproducibility of the PSPRP across different populations and clinical phenotypes.
153. Ko, J. H., Lee, C. S. & Eidelberg, D. Metabolic network expression in parkinsonism: clinical and dopaminergic correlations. *J. Cereb. Blood Flow. Metab.* **37**, 683–693 (2016).
154. Niethammer, M. et al. A disease-specific metabolic brain network associated with corticobasal degeneration. *Brain* **137**, 3036–3046 (2014).
155. Schindlbeck, K. A. et al. Neuropathological correlation supports automated image-based differential diagnosis in parkinsonism. *Eur. J. Nucl. Med. Mol. Imaging* **48**, 3522–3529 (2021).
This study compares the results of an automated pattern-based diagnostic algorithm with autopsy findings in patients with parkinsonism of uncertain cause.
156. Tripathi, M. et al. Automated differential diagnosis of early parkinsonism using metabolic brain networks: a validation study. *J. Nucl. Med.* **57**, 60–66 (2016).
157. Eckert, T. et al. FDG PET in the differential diagnosis of parkinsonian disorders. *Neuroimage* **26**, 912–921 (2005).
158. Meyer, P. T., Frings, L., Rücker, G. & Hellwig, S. ^{18}F-FDG PET in parkinsonism: differential diagnosis and evaluation of cognitive impairment. *J. Nucl. Med.* **58**, 1888–1898 (2017).
159. Gu, S.-C., Ye, Q. & Yuan, C.-X. Metabolic pattern analysis of ^{18}F-FDG PET as a marker for Parkinson's disease: a systematic review and meta-analysis. *Rev. Neurosci.* **30**, 743–756 (2019).
160. Manzanera, O. M. et al. Scaled subprofile modeling and convolutional neural networks for the identification of Parkinson's disease in 3D nuclear imaging data. *Int. J. Neural Syst.* **29**, 1950010 (2019).
161. Mudali, D., Teune, L. K., Renken, R. J., Leenders, K. L. & Roerdink, J. B. T. M. Classification of Parkinsonian syndromes from FDG-PET brain data using decision trees with SSM/PCA features. *Comput. Math. Methods Med.* **2015**, 136921 (2015).
162. Vázquez-Mojena, Y., León-Arcia, K., González-Zaldivar, Y., Rodríguez-Labrada, R. & Velázquez-Pérez, L. Gene therapy for polyglutamine spinocerebellar ataxias: advances, challenges, and perspectives. *Mov. Disord.* **36**, 2731–2744 (2021).
163. Fields, E. et al. Gene targeting techniques for Huntington's disease. *Ageing Res. Rev.* **70**, 101385 (2021).
164. van der Horn, H. J. et al. A resting-state fMRI pattern of spinocerebellar ataxia type 3 and comparison with ^{18}F-FDG PET. *Neuroimage Clin.* **34**, 103023 (2022).
165. Alzheimer's Association. 2018 Alzheimer's disease facts and figures. *Alzheimers Dement.* **14**, 367–429 (2018).
166. Hansson, O. Biomarkers for neurodegenerative diseases. *Nat. Med.* **27**, 954–963 (2021).
167. Yu, M., Sporns, O. & Saykin, A. J. The human connectome in Alzheimer disease — relationship to biomarkers and genetics. *Nat. Rev. Neurol.* **17**, 545–563 (2021).
168. Pievani, M., Filippini, N., Van Den Heuvel, M. P., Cappa, S. F. & Frisoni, G. B. Brain connectivity in neurodegenerative diseases — from phenotype to proteinopathy. *Nat. Rev. Neurol.* **10**, 620–633 (2014).
169. Pievani, M., de Haan, W., Wu, T., Seeley, W. W. & Frisoni, G. B. Functional network disruption in the degenerative dementias. *Lancet Neurol.* **10**, 829–843 (2011).
170. Raj, A., Kuceyeski, A. & Weiner, M. A network diffusion model of disease progression in dementia. *Neuron* **73**, 1204–1215 (2012).
Landmark paper relating network progression in neurodegenerative processes to pathological spread from one anatomical layer to the next.
171. Knopman, D. S. et al. Alzheimer disease. *Nat. Rev. Dis. Prim.* **7**, 33 (2021).
172. Karikari, T. K. et al. Blood phospho-tau in Alzheimer disease: analysis, interpretation, and clinical utility. *Nat. Rev. Neurol.* **42**, 400–418 (2022).
173. Badhwar, A. et al. Resting-state network dysfunction in Alzheimer's disease: a systematic review and meta-analysis. *Alzheimers Dement.* **8**, 73–85 (2017).
174. Scarmeas, N. et al. Covariance PET patterns in early Alzheimer's disease and subjects with cognitive impairment but no dementia: utility in group discrimination and correlations with functional performance. *Neuroimage* **23**, 35–45 (2004).
175. Devanand, D. P. et al. PET network abnormalities and cognitive decline in patients with mild cognitive impairment. *Neuropsychopharmacology* **31**, 1327–1334 (2006).
176. Teune, L. K. et al. The Alzheimer's disease-related glucose metabolic brain pattern. *Curr. Alzheimer Res.* **11**, 725–732 (2014).
177. Katako, A. et al. Machine learning identified an Alzheimer's disease-related FDG-PET pattern which is also expressed in Lewy body dementia and Parkinson's disease dementia. *Sci. Rep.* **8**, 13236 (2018).
178. Perovnik, M. et al. Identification and validation of Alzheimer's disease-related metabolic brain pattern in biomarker confirmed Alzheimer's dementia patients. *Sci. Rep.* **12**, 11752 (2022).
This study shows the diagnostic robustness of the ADRP across independent populations of patients with biologically confirmed Alzheimer disease.
179. Peretti, D. E. et al. Feasibility of pharmacokinetic parametric PET images in scaled subprofile modelling using principal component analysis. *Neuroimage Clin.* **30**, 102625 (2021).
180. Meles, S. K. et al. The Alzheimer's disease metabolic brain pattern in mild cognitive impairment. *J. Cereb. Blood Flow. Metab.* **37**, 3643–3648 (2017).
181. Blazhenets, G. et al. Principal components analysis of brain metabolism predicts development of Alzheimer dementia. *J. Nucl. Med.* **60**, 837–843 (2019).
182. Spetsieris, P. G., Ma, Y., Dhawan, V. & Eidelberg, D. Differential diagnosis of parkinsonian syndromes using PCA-based functional imaging features. *Neuroimage* **45**, 1241–1252 (2009).
183. Sörensen, A., Blazhenets, G., Schiller, F., Meyer, P. T. & Frings, L. Amyloid biomarkers as predictors of conversion from mild cognitive impairment to Alzheimer's dementia: a comparison of methods. *Alzheimers Res. Ther.* **12**, 155 (2020).
184. Blazhenets, G. et al. Predictive value of ^{18}F-florbetapir and ^{18}F-FDG PET for conversion from mild cognitive impairment to Alzheimer dementia. *J. Nucl. Med.* **61**, 597–603 (2020).
This study shows the value of the ADCRP cross-pattern as a predictor of dementia in patients with MCI.
185. Blazhenets, G. et al. Validation of the Alzheimer disease dementia conversion-related pattern as an ATN biomarker of neurodegeneration. *Neurology* **96**, e1358–e1368 (2021).
This study shows that the ADCRP outperforms fluid biomarkers of neurodegeneration as a predictor of dementia in patients with MCI.
186. Blum, D. et al. Controls-based denoising, a new approach for medical image analysis, improves prediction of conversion to Alzheimer's disease with FDG-PET. *Eur. J. Nucl. Med. Mol. Imaging* **46**, 2370–2379 (2019).
187. Blazhenets, G., Frings, L., Sörensen, A. & Meyer, P. T. Principal-component analysis–based measures of PET data closely reflect neuropathologic staging schemes. *J. Nucl. Med.* **62**, 855–860 (2021).
188. Li, T. R. et al. Exploring brain glucose metabolic patterns in cognitively normal adults at risk of Alzheimer's disease: a cross-validation study with Chinese and ADNI cohorts. *Neuroimage Clin.* **33**, 102900 (2022).
189. Tai, H. et al. The neuropsychological correlates of brain perfusion and gray matter volume in Alzheimer's disease. *J. Alzheimers Dis.* **78**, 1639–1652 (2020).
190. Ferreira, D., Nordberg, A. & Westman, E. Biological subtypes of Alzheimer disease. *Neurology* **94**, 436–448 (2020).
191. Jellinger, K. A. Pathobiological subtypes of Alzheimer disease. *Dement. Geriatr. Cogn. Disord.* **49**, 321–333 (2020).
192. Outeiro, T. F. et al. Dementia with Lewy bodies: an update and outlook. *Mol. Neurodegener.* **14**, 5 (2019).
193. Arnaoutoglou, N. A., O'Brien, J. T. & Underwood, B. R. Dementia with Lewy bodies — from scientific knowledge to clinical insights. *Nat. Rev. Neurol.* **15**, 103–112 (2019).
194. Iizuka, T. & Kameyama, M. Spatial metabolic profiles to discriminate dementia with Lewy bodies from Alzheimer disease. *J. Neurol.* **267**, 1960–1969 (2020).
195. Kang, S. W. et al. Implication of metabolic and dopamine transporter PET in dementia with Lewy bodies. *Sci. Rep.* **11**, 14394 (2021).
196. Perovnik, M. et al. Metabolic brain pattern in dementia with Lewy bodies: relationship to Alzheimer's disease topography. *Neuroimage Clin.* **35**, 103080 (2022).
197. Lu, J. et al. Consistent abnormalities in metabolic patterns of Lewy body dementias. *Mov. Disord.* **37**, 1861–1871 (2022).
198. McKeith, I. G. et al. Diagnosis and management of dementia with Lewy bodies: fourth consensus report of the DLB Consortium. *Neurology* **89**, 88–100 (2017).
199. Hepp, D. H. et al. Distribution and load of amyloid-β pathology in Parkinson disease and dementia with Lewy bodies. *J. Neuropathol. Exp. Neurol.* **75**, 936–945 (2016).
200. Lau, A. et al. Alzheimer's disease-related metabolic pattern in diverse forms of neurodegenerative diseases. *Diagnostics* **11**, 2023 (2021).
201. Ingram, M. et al. Spatial covariance analysis of FDG-PET and HMPAO-SPECT for the differential diagnosis of dementia with Lewy bodies and Alzheimer's disease. *Psychiatry Res. Neuroimaging* **322**, 111460 (2022).
202. Bang, J., Spina, S. & Miller, B. L. Frontotemporal dementia. *Lancet* **386**, 1672–1682 (2015).
203. Nazem, A. et al. A multivariate metabolic imaging marker for behavioral variant frontotemporal dementia. *Alzheimers Dement.* **10**, 583–594 (2018).
204. Rus, T. et al. Disease specific and nonspecific metabolic brain networks in behavioral variant of frontotemporal dementia. *Hum. Brain Mapp.* https://doi.org/10.1002/hbm.26140 (2022).
205. Filippi, M. et al. Functional network connectivity in the behavioral variant of frontotemporal dementia. *Cortex* **49**, 2389–2401 (2013).
206. Shlens, J. A tutorial on independent component analysis. Preprint at *arXiv* https://doi.org/10.48550/arXiv.1404.2986 (2014).
207. Myszczynska, M. A. et al. Applications of machine learning to diagnosis and treatment of neurodegenerative diseases. *Nat. Rev. Neurol.* **16**, 440–456 (2020).
Review of current applications of machine learning in the study of neurodegenerative diseases.
208. Young, A. L. et al. Uncovering the heterogeneity and temporal complexity of neurodegenerative diseases with subtype and stage inference. *Nat. Commun.* **9**, 4273 (2018).
209. Franzmeier, N. et al. Predicting sporadic Alzheimer's disease progression via inherited Alzheimer's disease-informed machine-learning. *Alzheimers Dement.* **16**, 501–511 (2020).
This study proposes a machine learning model to predict cognitive decline in individuals with autosomal dominant Alzheimer disease and amyloid-positive individuals with MCI using a combination of fluid and imaging biomarkers.
210. Davatzikos, C. Machine learning in neuroimaging: progress and challenges. *Neuroimage* **197**, 652–656 (2019).

211. Borchert, R. et al. Artificial intelligence for diagnosis and prognosis in neuroimaging for dementia; a systematic review. Preprint at *medRxiv* https://doi.org/10.1101/2021.12.12.21267677 (2021).

Acknowledgements
M.P. and T.R. were supported by the Slovenian Research Agency (ARRS) through grant P1-0389 and projects J7-2600 and J7-3150. T.R. is a recipient of the Fulbright Foreign Student Program sponsored by the US Department of State's Bureau of Educational and Cultural Affairs. The authors thank Yoon Young Choi for her invaluable editorial assistance in preparing the manuscript.

Competing interests
D.E. declares that he receives funding from the NIH and The Michael J. Fox Foundation for Parkinson's Research.

Author contributions
All authors researched data for the article, contributed substantially to the discussion of content, wrote the article and reviewed and/or edited the manuscript before submission.

Additional information
Correspondence should be addressed to David Eidelberg.

Peer review information *Nature Reviews Neurology* thanks Yoshikazu Nakano, who co-reviewed with Shigeki Hirano; Meichen Yu; and the other, anonymous, reviewer(s) for their contribution to the peer review of this work.